DISTRIBUTION OF SLEEP STRUCTURE IS MAINTAINED, BUT ADJUSTED IN AN ACUTE CIRCADIAN SHIFT: A STUDY BY CONTINUOUS LONG-TERM LOCAL FIELD POTENTIAL RECORDING

RYAN Y. ROTA
BSc. University of Lethbridge, 2009

A Thesis
Submitted to the School of Graduate Studies
of the University of Lethbridge
in Partial Fulfillment of the
Requirements for the Degree

MASTER OF SCIENCE

Department of Neuroscience
University of Lethbridge
LETHBRIDGE, ALBERTA, CANADA

DISTRIBUTION OF SLEEP STRUCTURE IS MAINTAINED, BUT ADJUSTED IN AN ACUTE CIRCADIAN SHIFT: A STUDY BY CONTINUOUS LONG-TERM LOCAL FIELD POTENTIAL RECORDING

RYAN ROTA

Date of Defense: August 06, 2014

Dr. Masami Tatsuno……....Associate Professor……..Ph.D.
Co-Supervisor

Dr. Robert McDonald……..Professor……. Ph.D.
Co-supervisor

Dr. Bruce McNaughton……Professor……..... Ph.D.
Thesis Examination Committee member

Dr. Robert Sutherland……..Professor……..… Ph.D.
Thesis Examination Committee member

Dr. Robbin Gibb……...Professor……..…….. Ph.D.
Chair, Thesis Examination Committee member

Abstract

Evidence suggests that the disruption of circadian rhythms has a negative impact on memory retention. It is therefore speculated that circadian disruption influences some property of sleep responsible for memory retention, but little is known about this relationship. In order to investigate this question, we have continuously recorded local field potentials in the hippocampus and prefrontal cortex of freely behaving adult male Long Evans rats. The current analysis indicates that daily quantities of sleep are strongly maintained in an acute circadian shift. Furthermore, hourly sleep distributions are largely maintained during the shift. Contrastingly, an acute circadian shift is able to alter the hourly distribution of vigilance states and sleep based events predominantly across pre-entrainment to post-entrainment, supporting previous findings of memory retention deficits observed during post-entrainment but not shifting epochs. Furthermore, current analysis suggests that pre-entrainment hourly distributions are conserved, but relocated in phase with post-entrainment.

Acknowledgements

I would like to send a well-deserved thank you my supervisors Dr. Masami Tatsuno and Dr. Robert McDonald for their exceptional guidance, patience, ideas, knowledge and commitment to developing this thesis. It has been an honour to be your student. Thank you to Dr. Bruce McNaughton for his support throughout my graduate work, Dr. Robbin Gibb for her inspiration and chairing my committee, and Dr. Robert Sutherland for sitting on my thesis committee. Also, I would like to especially thank Hendrik Steenland and Karim Ali for their friendship and countless hours spent helping me develop skills in their respective specialized fields.

Thank you to all the members of the Tatsuno and McDonald labs that have worked with me to exchange and develop ideas. Of the Tatsuno lab, I would like to specifically thank Michael Eckert for allowing me to ask and answering countless questions. Thank you to all members of the CCBN and Polaris Group for creating an outstanding learning environment for neuroscience research. Thank you also to the independent study students Megan Bach, Matthew Harrison, Stephen Tkach, and Tyler Morton for your excellent help.

Thank you also to my family and friends for providing me with joy and encouragement throughout my academic career.

Ryan Rota
The University of Lethbridge
August, 2014

Table of Contents

List of Tables

List of Figures

List of Abbreviations

REM	Rapid eye movement
MWM	Morris water maze
LFP	Local field potential
LVS	Low voltage spindle
AWG	American wire gauge
EMG	Electromyogram
KW	Kruskal-Wallis
MC	Multiple Comparisons
non-ZT	non-Zeitgeber time
ZT	Zeitgeber time
SEM	Standard error of the mean
SWR	Sharp wave ripple
LTP	Long term potentiation
LTD	Long term depression
CREB	cAMP-responsive element-binding protein
PER	Period clock gene

1. Introduction

Circadian cycles govern regular waking and sleeping patterns in our daily lives. Mechanisms regulating circadian cycles can be altered through biological and behavioural changes. Circadian disruption is commonly experienced by aging populations and shift workers. It has also been reported that circadian rhythms are markedly disturbed in Alzheimer's disease patients (Witting et al., 1990;Volicer et al., 2001). Increasing evidence also indicates that there is a close link between circadian disruption and cognitive impairment. For example, Craig and McDonald (2008) have demonstrated that a 64 day chronic circadian disruption paradigm, caused by photic (i.e. light) phase shifting, is correlated with a deficit in both the acquisition and retention of a spatial memory when tested on the Morris water maze (MWM). Devan et al. (2001) have also illustrated that six days of acute circadian disruption obstructed the long term retention, but not acquisition of a MWM platform location, when tested seven and seventeen days later. Despite these findings, there is little understanding of the physiological mechanisms responsible for an impairment of the retention and acquisition of spatial memories, in a circadian disruption paradigm. As a first step to understanding the observed impairments in memory retention, but not acquisition (Devan et al., 2001), this study aims to investigate how an acute circadian phase shift modifies the structure of sleep. In the current study, we have focused sleep because it has been shown to play an important role in learning and memory.

Sleep is described as a loss of behavioural control and consciousness (Diekelmann and Born, 2010), which is closely regulated by both circadian and homeostatic mechanisms (Cirelli, 2009) and has been shown to enhance the consolidation

of new memories (Diekelmann and Born, 2010). A sleeping state can be broadly categorized into vigilance states known as rapid eye movement (REM) sleep and non-REM sleep. REM and non-REM vigilance states can be classified using local field potentials (LFPs) generated by the flow of electrical current, structured by synaptic activity or muscle tone. REM sleep is marked as a period of muscle atonia which is pronounced by hippocampal theta oscillations (5-10 Hz). Cortical activity during REM sleep and waking behaviour can be described as desynchronized (i.e. showing an LFP bearing a low voltage high frequency state). Conversely, a non-REM sleep state gives rise to cortical delta activity (1-4 Hz) and has been shown to increase in relation to the amount of prior waking activity in both human and rat studies (Tobler and Borbely, 1986;Dijk et al., 1987;Lancel et al., 1991;Deboer and Tobler, 2003). It is hypothesized that REM sleep contributes to memory consolidation (Karni et al., 1994;Rasch and Born, 2013), and more specifically procedural memories (Smith, 1995). Declarative memory consolidation has also been shown to benefit from periods of non-REM sleep (Barrett and Ekstrand, 1972;Kudrimoti et al., 1999;Plihal and Born, 1999), which are consequently enriched with delta power. Furthermore, sleep can be characterized into distinctive events using LFPs.

The present study additionally explores how two non-REM based events, spindles and k-complexes, are modified by acute circadian disruption. Spindle activity (approximately 10-15Hz) observed in the primary sensory and prefrontal areas of the cortex are generated in the thalamus, and projected to the cortex through bursting thalamo-cortical cells (Luthi, 2013). Both human (Gais and Born, 2004) and rodent (Eschenko et al., 2006) studies have shown increased spindle density after a learning

experience. K-complexes contain frequencies in the delta range, which occur rhythmically (<1 Hz), and are the product of synchronous excitation of cortical neuronal populations followed by neuronal hyperpolarization (Amzica and Steriade, 2002). Cortical k-complexes are able to trigger spindling, through connections from the cortex to the thalamic reticular nucleus and thalamo-cortical activation (Amzica and Steriade, 2002). Johnson et al. (2010) have positively correlated stored-trace reactivation to the density of cellular population down-to-up state transitions, k-complex and low voltage spindle (LVS) events observable in LFPs. Currently, it is not known how spindles and k-complex events are modified over the course of an acute circadian shift. We therefore hypothesize that an acute circadian shift causes the disruption of a critical property of sleep or sleep based event.

The negative effect of circadian disruption on memory based task performance has been investigated by several groups (Tapp and Holloway, 1981;Fekete et al., 1985;Antoniadis et al., 2000;Cho et al., 2000;Devan et al., 2001;Craig and McDonald, 2008). However the effects of acute circadian disruption on sleep structure have not been largely investigated. The role sleep plays in memory consolidation solicits the question of whether acute circadian disruption is able to modify properties of sleep. In order to examine this question we have performed continuous LFP recordings in freely behaving rats that were exposed to acute circadian disruption. By subjecting the rats to an acute phase shift and continuously monitoring their LFPs, we are able to explore the effects of circadian disruption on their delta power and vigilance states. The present study is also able to continuously measure changes to cortical k-complexes and spindles. This unique

data set has allowed us to examine the quantity and distributions of these properties, and their long term relationship to an acute circadian shift.

2. Materials and Methods

2.1 Subjects

Two groups of eight naive six month old male nocturnal Long-Evans hooded rats were surgically implanted with LFP electrodes. After surgical implantation the rats were given one to two weeks of recovery time before being permanently housed in the recording cages. The subjects had food and water available *ad libitum* during the recovery period and once placed into the recording cages; additionally gaining access to a running wheel in the recording cages. Six of the eight implanted rats were selected to be permanently placed into the recording housing units. Selection of these six rats was determined by continuously monitoring individual rat LFP stability and quality for a period of 3-4 weeks. The rats were handled daily prior to surgery, monitored during recovery and handled daily while housed in the recording cages prior to beginning the experimental recording. Once the recording had begun rats were not contacted unless recording equipment adjustments were necessary. Apart from recording corrections, the recording room was only entered for scheduled cage tray cleaning coupled with food and water replacement.

2.2 Animal housing

Six housing units were constructed, allowing the rats to continuously live in a recording environment for the entirety of the experiment. These units were built to resolve issues surrounding 24 hour/day recording in a freely moving rat and the electrostatic nature of traditional rat cages (plastic), which can reduce the quality of electrophysiological data collected. The housing units were made of an aluminum frame in which tempered glass is inserted to create a 40 x 40 x 40 cm box. A bedding tray was

placed at the bottom of the box and could be easily removed horizontally for cleaning. The roof was made of aluminum as well with two large holes. The first hole allowed the wire tether from the commutator to connect the rat in the housing box and the second hole allowed for a mounted a Blue Cherry video camera (supplemental Figure 15) used to monitor rat behavior. On the inside back wall of the unit, a running wheel was attached to a single spindle. The diameter of the wheel was 30.5 cm. Four holes in the glass side panels (two holes in two panels) were used to mount a water bottle and a food bin system to hold the bottle on the outside of the box and the food bin on the inside of the box.

2.3 Data Acquisition

For the first group of six rats, a first generation Avatar system (Avatar EEG Solutions, Calgary, CA) was adapted for rat use. This system was capable of recording at a 256Hz sampling rate with up to six referenced channels, Bluetooth real-time transmission rate of 256Hz, 16bit sample size and a 6.5mV dynamic range. The second group of six rats were recorded on a new Avatar 3000 (Avatar EEG Solutions, Calgary, CA) series having a sampling rate of 2000Hz (recorded to an internal microSD card, which were replaced weekly and used for offline analysis), 250Hz Bluetooth transmission (used for continuously monitoring LFP activity from a remote location), 24 bit sample size and 2.25V dynamic range. Live LFP recordings were viewed (supplemental Figure 16) using freely available open source EDF Browser software (Beelen). An assembly of rat housing, Blue Cherry digital video recording system, and Avatar EEG recording systems (Figure 1.1) were used to monitor rat behaviour, running wheel activity and, LFP activity.

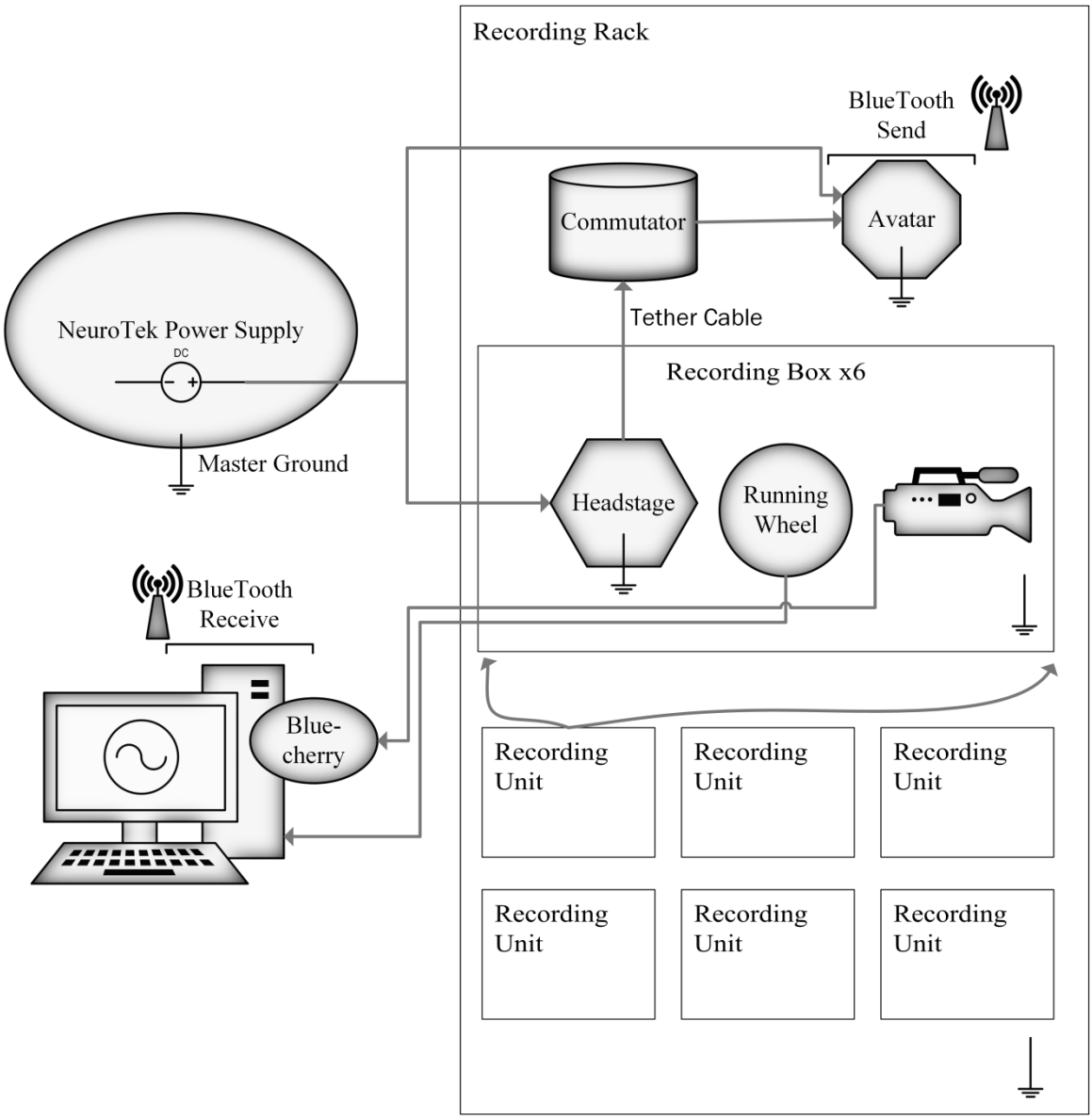

Figure 1.1. Recording system schematic of parallel six animal system, used to monitor local field potentials in the current experiment. Blue tooth LFP recordings were transmitted wirelessly to the recording system. Both running wheel activity and Blue Cherry video recording systems were transmitted via coaxial cable to a recording computer. A NeuroTek power supply was used to power both the Avatar recording systems and Neurotek headstages. All recording rack, recording box, animal headstage, and Avatar systems were grounded to the master ground of the NeuroTek power supply.

2.4 Electrode and surgical protocol

Twisted pairs of bipolar electrodes consisting of medical grade 40 AWG (American wire gauge) stainless steel wire coated in polytetrafluoroethylene (Teflon) were constructed for surgical implantation. Pre-surgery electrode impedances were tested and range from 50K to 100K ohms; once implanted, signal producing electrode to rat tail impedances ranged from 150K to 400K ohms. Three pairs of electrodes were implanted in the hippocampus (-3.84mm from Bregma, 2.4mm lateral and 2.4mm depth; tip separation of 0.4mm), pre-frontal cortex (2.76mm from Bregma, 2.8mm lateral and 4.25mm depth at a 55^{o} angle from dura; tip separation of 1.8mm), and an EMG (electromyogram) sutured bilaterally to the Acromiotrapezius muscle. Depth and positions of electrodes were confirmed by histological analysis. A single stainless steel ground screw was also implanted in each rat's cranium (-2mm from Lambda).

2.5 Circadian shift

Each group of six selected rats were placed in the recording housing environment two months prior to beginning the recording and maintained on a 12:12-h dark:light (2 lux and 320 lux respectively) cycle, consisting of lights off at 9am and on at 9pm. Wheel running, neck muscle EMG, HC and PFC LFP activity was monitored during this period to confirm the rats had entrained to the 12:12-h dark:light cycle. A period of 6 days preceding the acute phase shift constituted the pre-entrainment epoch of the protocol. The rats were exposed to an acute phase shift implemented by advancing the rat's dark phase by three hours each day for six days (Devan et al., 2001), whereby advancing the subjective time of the rat by three hours each day. The post-entrainment epoch is composed of a period where the rats were re-entrained for 6 days on a 12:12-h dark:light

cycle (Table 1), which has been maintained at a 3 hour phase delay when compared to pre-entrainment.

We have used the current model of acute circadian disruption (Table 1) because it has been implicated in memory retention deficits (Devan et al., 2001). Variations on this model of circadian disruption have shown disruption of memory retention in a passive avoidance task (Tapp and Holloway, 1981;Fekete et al., 1985). Furthermore the final 3-hour maintained advancement in post-entrainment allows us to examine the effect of a maintained light/dark cycle advance in post-entrainment, when compared to pre-entrainment. With this manipulation we are able to observe whether sleep structure changes are observable during incremental 3-hour dark phase advances or during maintained light/dark exposure.

Day	Light off – Light on
Pre-Entrainment (6 days)	9:00 – 21:00
Shift Day 1	6:00 – 18:00
Shift Day 2	3:00 – 15:00
Shift Day 3	0:00 – 12:00
Shift Day 4	21:00 – 9:00
Shift Day 5	18:00 – 6:00
Shift Day 6	15:00 – 3:00
Post-entrainment (6 days)	12:00 – 0:00

Table 1. Acute circadian shift schedule of dark phase advance used to induce acute circadian disruption.

2.6 Offline sleep scoring and data analysis

Analysis was focused around six days of pre-entrainment, six days of acute phase shift and six days of post-entrainment. All analysis has been performed on 18 days of continuously record local field potential recordings. EMG was filtered between 10-50Hz and a movement threshold of 1.5*median of the EMG signal was chosen to detect motionless epochs (indicative of sleep); verified manually with video referenced scoring. In order to reduce fragmentation of sleep detection, motionless fragments were merged within three seconds of each other; sleep epochs less than 30 seconds in length were also removed. Theta and delta were obtained (5.5-10Hz and 1-4.5 Hz respectively) from hippocampal CA1 recordings and applied to REM detection. REM epochs were found by calculating when a ratio of theta to delta power exceeded a threshold of the 80^{th} percentile of the overall theta to delta power ratio during a motionless epoch (Figure 1.2). REM fragmentation was also limited by merging REM epochs that occur within 40 seconds of each other; REM epochs less than 30 seconds in length were removed. Non-REM epochs were calculated by subtracting REM sleep from motionless epochs.

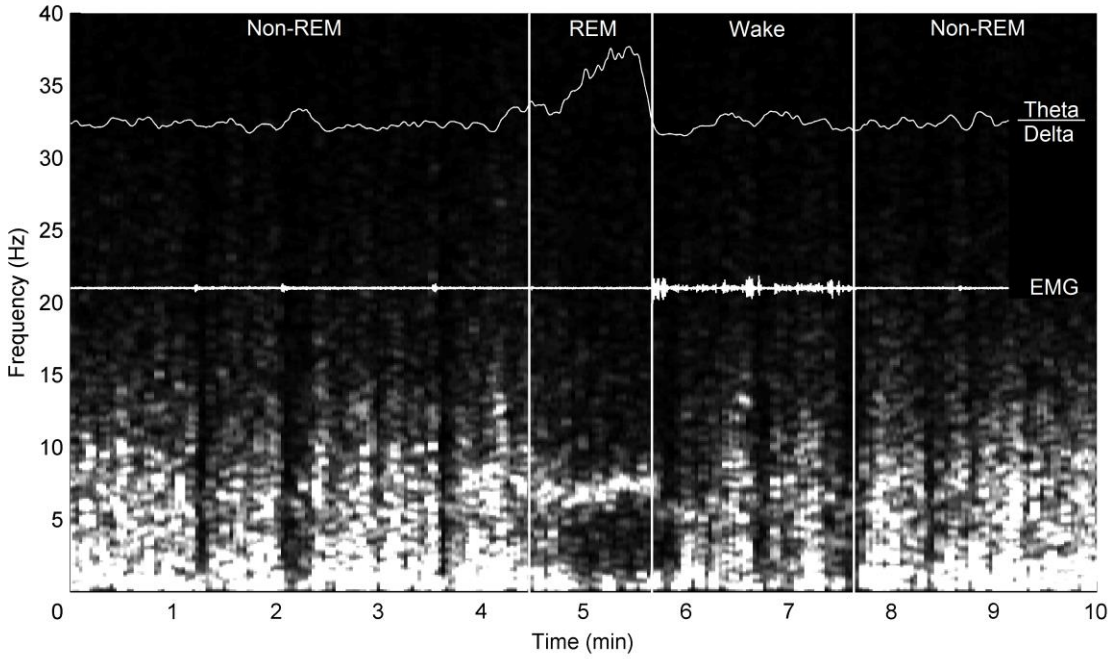

Figure 1.2. Vigilance state detection; illustrative sample of a hippocampal spectrogram showing segmentation of REM, non-REM, and waking.

A 10-20Hz filter was used during motionless epochs for LVS detection. To improve quality and continuity of LVS detection a minimum distance between LVS and minimum duration of LVS (700ms and 200ms respectively) was imposed. Thresholding of three standard deviations was then set to detect LVS using the power of the filtered cortical LFP (Figure 1.3). K-complex detection was performed by filtering the cortical LFP trace between 0.75Hz and 6Hz. The slope of the filtered signal was then computed and a large negative slope (99.5 percentile) followed by a reduced positive slope (98 percentile) were used as criteria for K-complex detection; the start and end point of the K-complex was determined when the slope of the filtered cortical trace crossed zero before and after the point of detection respectively (Figure 1.3). In summary, analysis algorithms have been used to create clearly defined start and end times for motionless, non-REM, REM, non-motionless, LVS, and k-complex events (Figure 1.4).

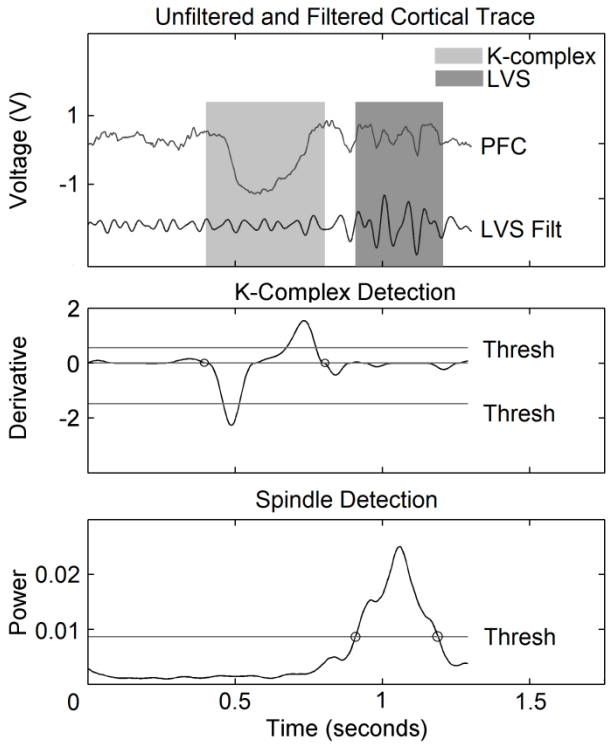

Figure 1.3. K-complex and LVS detection. Depicted in the uppermost subplot are unfiltered cortical trace (PFC) and offset filtered trace (LVS Filt) for LVS (10-20Hz), a derivative of the PFC trace filtered for k-complexes (0.75-6 Hz) is shown in the middle subplot, smoothed absolute values of the PFC trace filtered for LVS are illustrated in the bottommost subplot (‘o’ marks the beginning and end of detected k-complex and spindle).

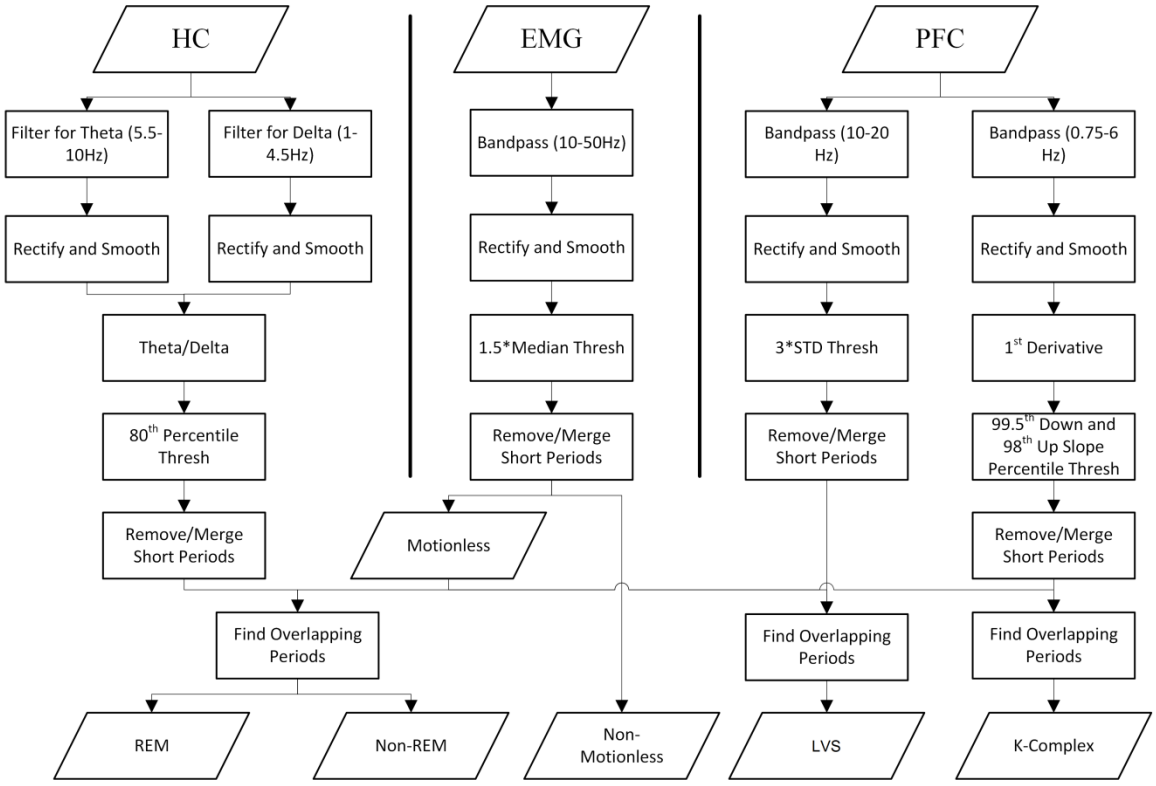

Figure 1.4. Offline automated vigilance state and sleep event detection algorithm used to select epoch start and end times for REM, non-REM, motionless, non-motionless, LVS, and k-complex events. Data sets obtained from LFP recordings in the HC, PFC, and EMG.

2.7 Statistical analysis

Analyses were performed on eight rats for motionless, REM and non-REM, and seven rats for k-complex and spindle comparisons (10 rats total; five rats were included in all analyses, an additional 3 and 2 rats were included in each respective analysis group). Rats were selected for analysis based on long term recording fidelity and quality. A Kruskal-Wallis (KW) test (non-parametric ANOVA) was used to determine statistically significant differences in the structure of motionless, non-REM, REM, LVS, and K-complex events across six days of pre-entrainment, shift, and post-entrainment epochs (18 days total). Once these differences were established, a multiple comparisons (MC) procedure using the Tukey-Kramer method, was implemented to determine the identity of the pairs found to be significantly different in the KW test. Further investigation into the distribution of vigilance states between epochs (pre-entrainment, shift and post-entrainment) and across days required a Pearson's linear correlation coefficient.

3. Results

In order to investigate changes to sleep structure we first looked at daily (per day) quantities of motionless, non-REM, REM, LVS density, and k-complex density events comparing daily mean value across pre-entrainment, shift, and post-entrainment epochs. This basic measurement allows us to investigate whether or not any large scale changes occur to the aforementioned variables between pre-entrainment, shift, and post-entrainment epochs. We then conducted a more detailed investigation into changes to the hourly (per hour) distribution of delta power (Figure 1.5) and previously examined per day sleep characteristics across pre-entrainment, shift, and post-entrainment epochs. After establishing individual daily quantities and hourly density distributions of k-complex and LVS events we explored properties of the relative timing between k-complex and spindle onsets. Hourly distributions were compared using non-zeitgeber (non-ZT) and adjusted zeitgeber time (ZT) values for circadian phase alignment between pre-entrainment and post-entrainment epochs. This was accomplished by implementing a 3-hour phase advance in pre-entrainment, whereby matching pre-entrainment with post-entrainment light/dark phases.

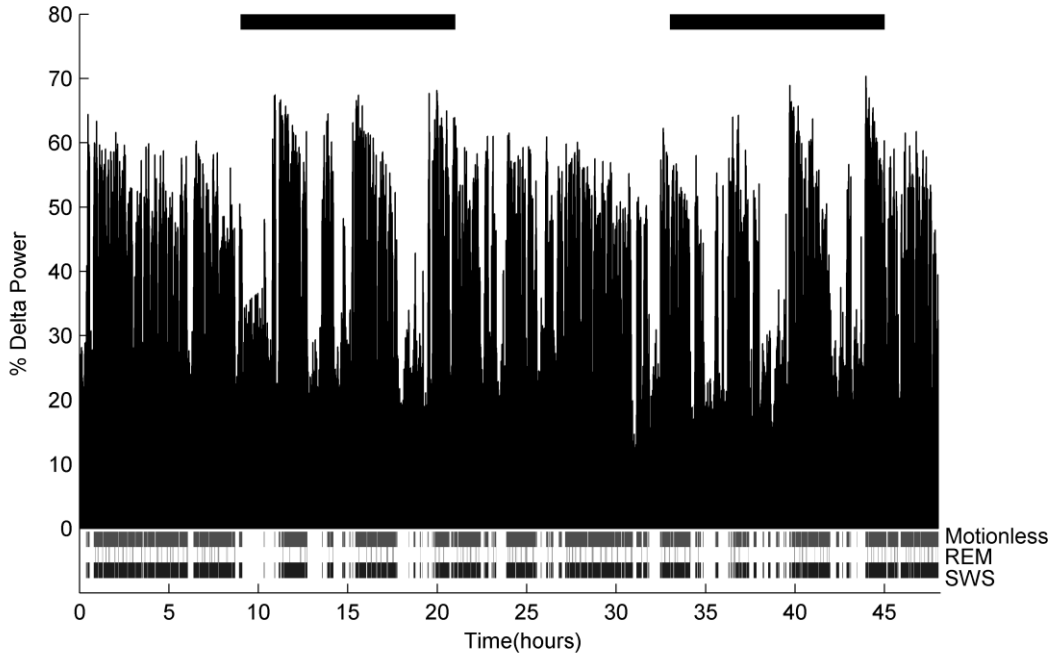

Figure 1.5. Delta distribution depicting current day to next day (48 hours) delta power (1-4.5Hz, normalized as a percentage of total power and binned over 1 min) distribution during the pre-entrainment period of the recording for one representative rat. Detected motionless (M), REM (R) and non-REM (S) vigilance states epochs depicted in lower section of figure. Upper section contains black bars depicting dark phase of lights schedule. A build-up of delta power was shown in the rats during waking behaviour, which declined during the following sleep session. Delta power distribution has shown steep increases followed by a decline during individual motionless periods, as well as an overall decline during lights on.

3.1 No change to the distribution of delta power per hour

The hourly percentage of delta power was tested using a KW test ($P < 0.05$) across pre-entrainment, shift and post-entrainment periods. If a significant difference was found using the KW test ($P < 0.05$), a MC ($P<0.05$ and $P<0.01$) test was performed. No significant difference was found between the distribution of pre-entrainment, shift, and post-entrainment of hourly delta power (Figure 2.1) when tested using a KW test ($P<0.05$). No significant modifications were observed when comparing adjusted ZT values (Figure 2.2) when compared across pre-entrainment, shift and post-entrainment epochs, using a KW ($P<0.05$).

2.1

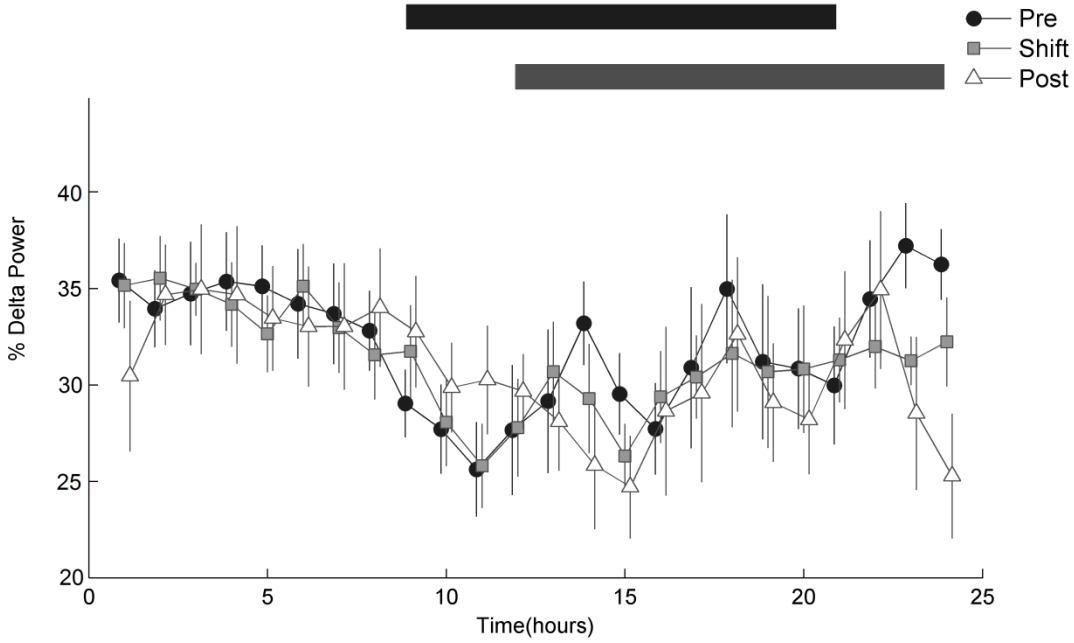
Pre
Shift
Post
% Delta Power
40
35
30
25
20
0
5
10
15
20
25
Time(hours)

2.2

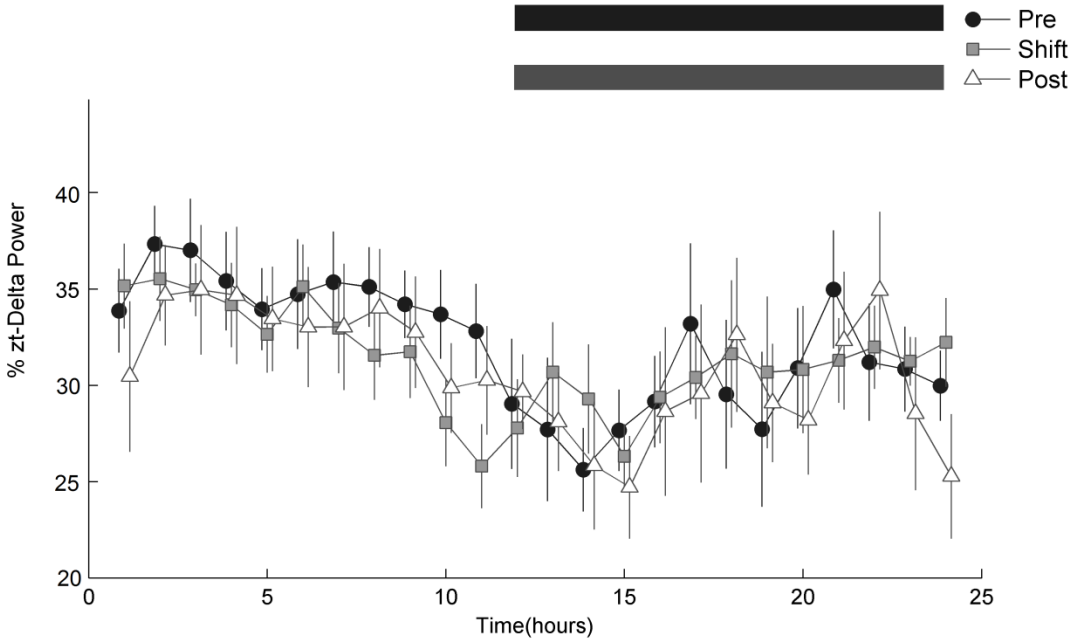
Pre
Shift
Post
% zt-Delta Power
40
35
30
25
20
0
5
10
15
20
25
Time(hours)

Figure 2. Daily distribution of hourly delta power examined over a 24 hour period in both **2.1)** non-ZT and **2.2)** ZT adjusted light/dark phases. Binned one minute ratios of delta divided by total spectrum power were taken for individual rats, delta power was then then averaged over 60 bins for each hour mark (plotted points shifted by +/- 0.15 hours for clarity). Mean delta power across rats (n = 7), is averaged and standard error of the mean (SEM) for each hour across the 6 days of pre-entrainment, shift, and post-entrainment is plotted (vertical error bars). Upper section contains black bars depicting dark phase of pre-entrainment and post-entrainment. Statistical significance testing ($P < 0.05$) was done using the KW and MC test across pre-entrainment to shift, shift to post-entrainment, and pre-entrainment to post-entrainment epochs.

3.2 No change to the quantity of motionless, non-REM, and REM per day

The daily percent of time, number and average length of non-REM, REM, and motionless vigilance states were tested using a KW test ($P < 0.05$) across pre-entrainment, shift and post-entrainment periods. If a significant difference was found using the KW test ($P < 0.05$), a MC ($P<0.05$ and $P<0.01$) test was performed. Figures 3.1, 3.4, and 3.7 show no changes to the percent of time spent in motionless, non-REM, and REM vigilance states per day compared when tested using a KW test ($P <0.05$) across pre-entrainment, shift, and post-entrainment epochs. Figure 3.2, 3.5, 3.8 indicate no change to the number of motionless, REM, and non-REM epochs per day when tested using a KW test ($P <0.05$) across pre-entrainment, shift, and post-entrainment epochs. Figure 3.3 3.6, 3.9 indicate no change to the mean length of motionless, REM, and non-

REM epochs per day when tested using a KW test ($P < 0.05$) across pre-entrainment, shift, and post-entrainment epochs.

3.1

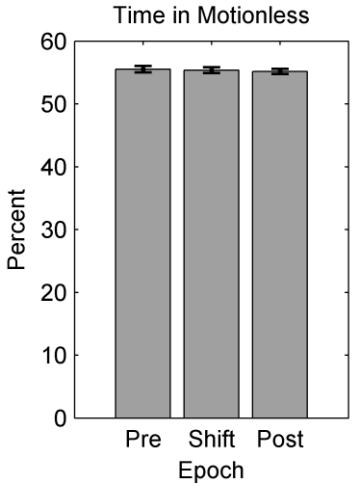

3.2

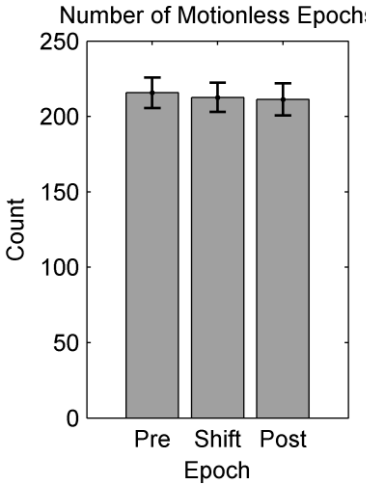

3.3

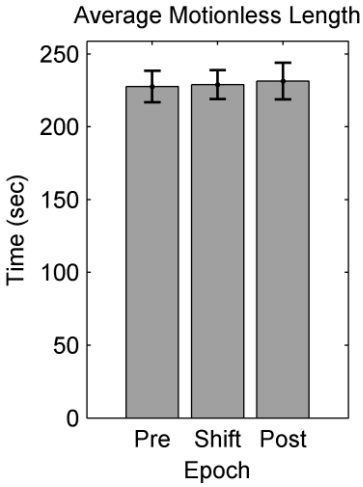

3.4

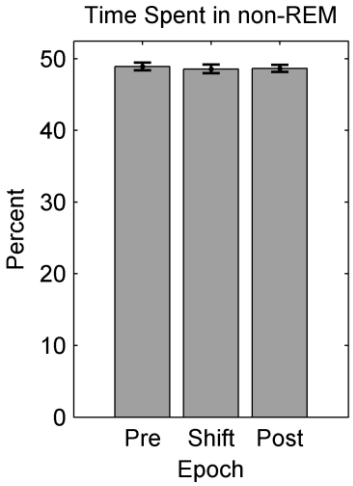

3.5

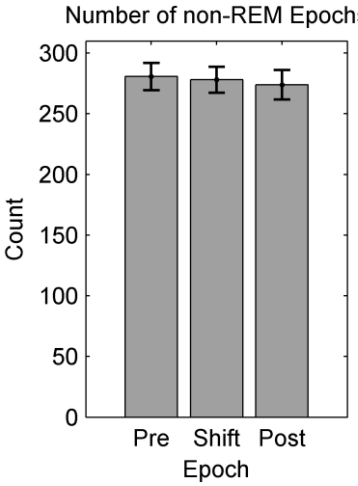

3.6

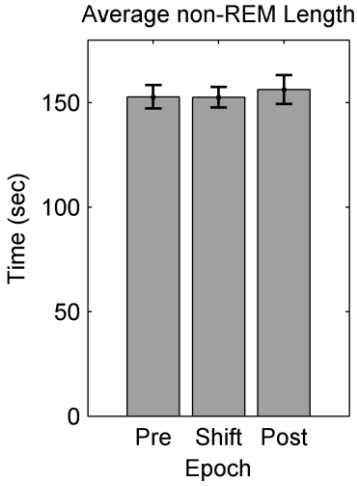

3.7

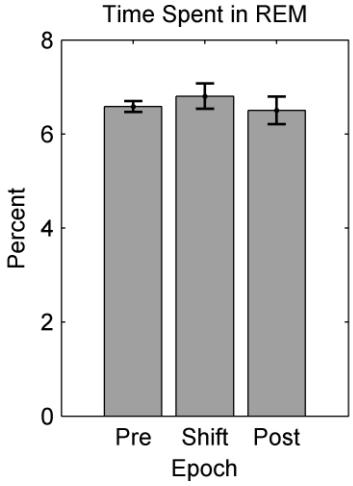

3.8

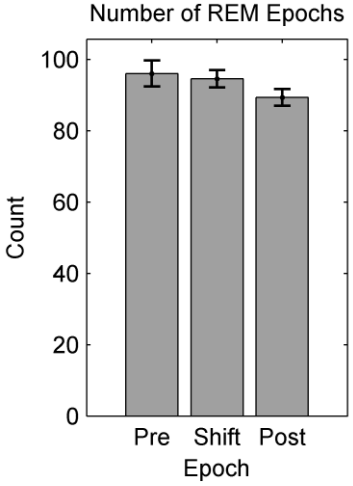

3.9

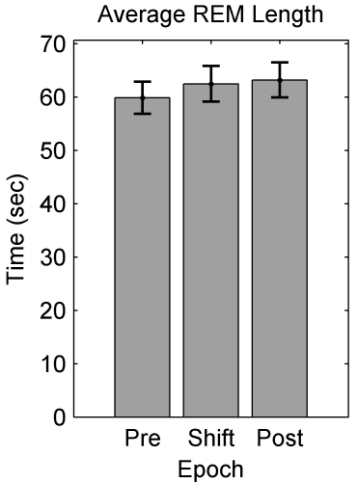

Figure 3. Mean daily quantities of vigilance states (i.e. motionless, non-REM, and REM) across 6 days of pre-entrainment, shift, and post-entrainment epochs. Vertical error bars represent SEM when comparing mean values amongst rats (n=8) of each day across 6 days of pre-entrainment, shift and post-entrainment. Statistical significance was tested using a KW and MC test ($P < 0.05$). **3.1, 3.4, 3.7)** Percent of the total amount of time for each day spent in vigilance states. **3.2, 3.5, 3.8)** Number of vigilance states. **3.3, 3.6, 3.9)** Mean length of individual vigilance states.

3.3 Modification to the distribution of motionless, non-REM, and REM per hour

A KW ($P<0.05$) and MC ($P<0.05$ and $P<0.01$) test was used to test significant changes of hourly motionless, non-REM, REM epoch distributions across pre-entrainment, shift, and post-entrainment periods. Significant changes have been found when comparing the percent of time spent in motionless across pre-entrainment to post-entrainment of hours 9, 10, 11 and 24 (KW $P<0.05$ and MC $P_{pre\text{-}post} < 0.01$, Figure 4.1) and pre-entrainment to shift of hour 10 (KW $P<0.05$ and MC $P_{pre\text{-}shift} < 0.05$, Figure 4.1). Motionless ZT shifted values show a significant effect between pre-entrainment to post-entrainment of hour 5 (KW $P<0.05$ and MC $P_{pre\text{-}post} < 0.05$, Figure 4.2), pre-entrainment to shift of hour 11 (KW $P<0.05$ and MC $P_{pre\text{-}shift} < 0.01$, Figure 4.2), hour 10 and 24 (KW $P<0.05$ and MC $P_{pre\text{-}shift} < 0.05$, Figure 4.2), and shift to post-entrainment of hour 24 (KW $P<0.05$ and MC $P_{shift\text{-}post} < 0.05$, Figure 4.2). Significant modifications were found to the percent of time spent in non-REM sleep across pre-entrainment to post-entrainment of hours 9, 10, 11 (KW $P<0.05$ and MC $P_{pre\text{-}post} < 0.01$, Figure 4.3) and hour 24 (KW $P<0.05$ and MC $P_{pre\text{-}post} < 0.05$, Figure 4.3). When comparing non-REM ZT shifted values, significant modifications were found between

pre-entrainment to shift epochs on hour 11 (KW $P<0.05$ and MC $P_{pre\text{-}shift} < 0.01$, Figure 4.4), hours 6, 9, and 24 (KW $P<0.05$ and MC $P_{pre\text{-}shift} < 0.05$, Figure 4.4), and pre to post-entrainment of hour 5 (KW $P<0.05$ and MC $P_{pre\text{-}post} < 0.05$, Figure 4.4). Significant changes were found to the percent of time spent in REM sleep across pre-entrainment to post-entrainment of hours 10, 24 (KW $P<0.05$ and MC $P_{pre\text{-}post} < 0.01$, Figure 4.5), 1, 11, 12 (KW $P<0.05$ and MC $P_{pre\text{-}post} < 0.05$, Figure 4.5) and shift to post-entrainment of hour 1 (KW $P<0.05$ and MC $P_{shift\text{-}post} < 0.05$, Figure 4.5). When comparing REM ZT shifted values significant modification were found between pre-entrainment to shift of hour 11 (KW $P<0.05$ and MC $P_{pre\text{-}shift}< 0.01$, Figure 4.6), hours 19 and 24 (KW $P<0.05$ and MC $P_{pre\text{-}shift} < 0.05$, Figure 4.6), shift to post-entrainment of hour 1 (KW $P<0.05$ and MC $P_{shift\text{-}post} < 0.01$, Figure 4.6), and pre-entrainment to post-entrainment of hour 19 (KW $P<0.05$ and MC $P_{pre\text{-}post} < 0.05$, Figure 4.6). These results indicate the hourly distribution of motionless, non-REM, and REM vigilance states were predominantly modified between pre-entrainment to post-entrainment epochs in non-ZT adjusted epochs (Figure 4.1, Figure 4.3, and Figure 4.5), which are restored with a ZT shift (Figure 4.2, Figure 4.4, and Figure 4.6). Indicating the maintained post-entrainment light/dark cycle significantly modified hourly distributions when compared to pre-entrainment.

4.1

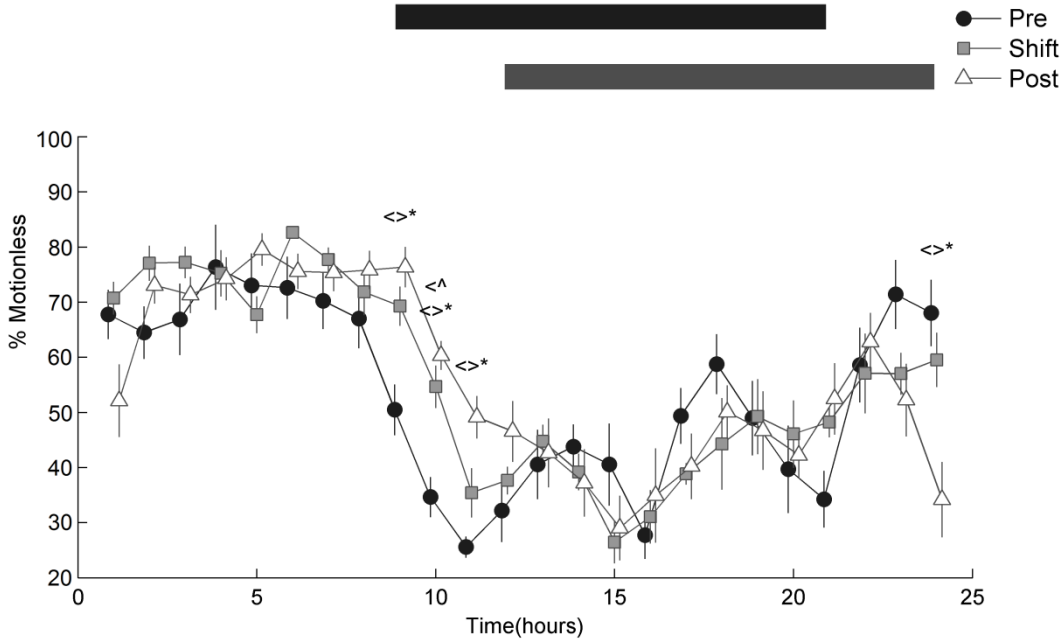
Pre
Shift
Post
% Motionless
Time(hours)
<>*
<^
<>*
<>*
<>*

4.2

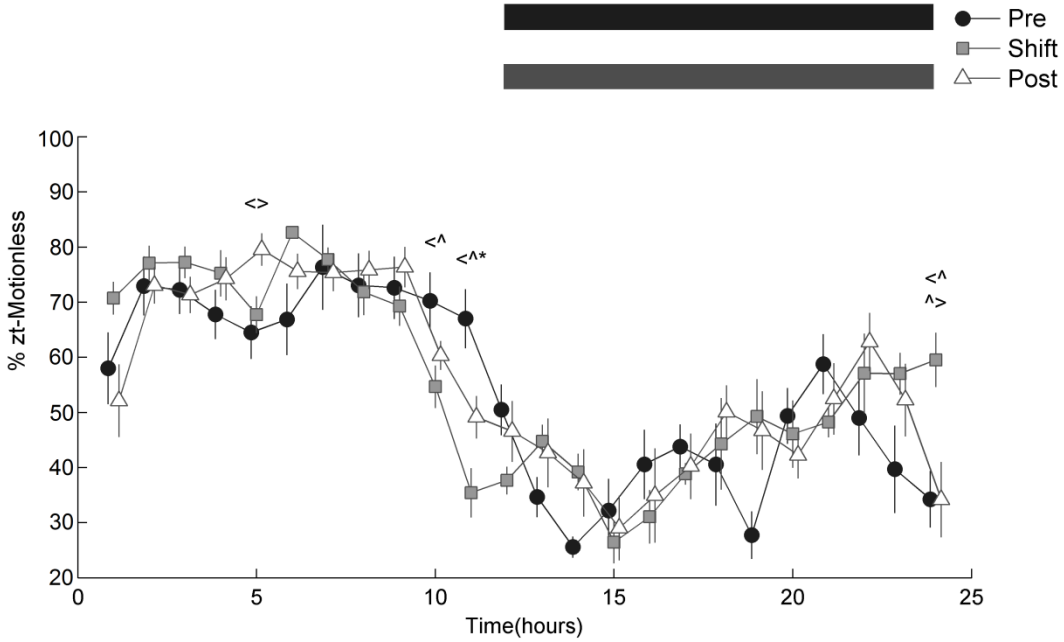
Pre
Shift
Post
% zt-Motionless
Time(hours)
<>
<^
<^*
<^
^>

4.3

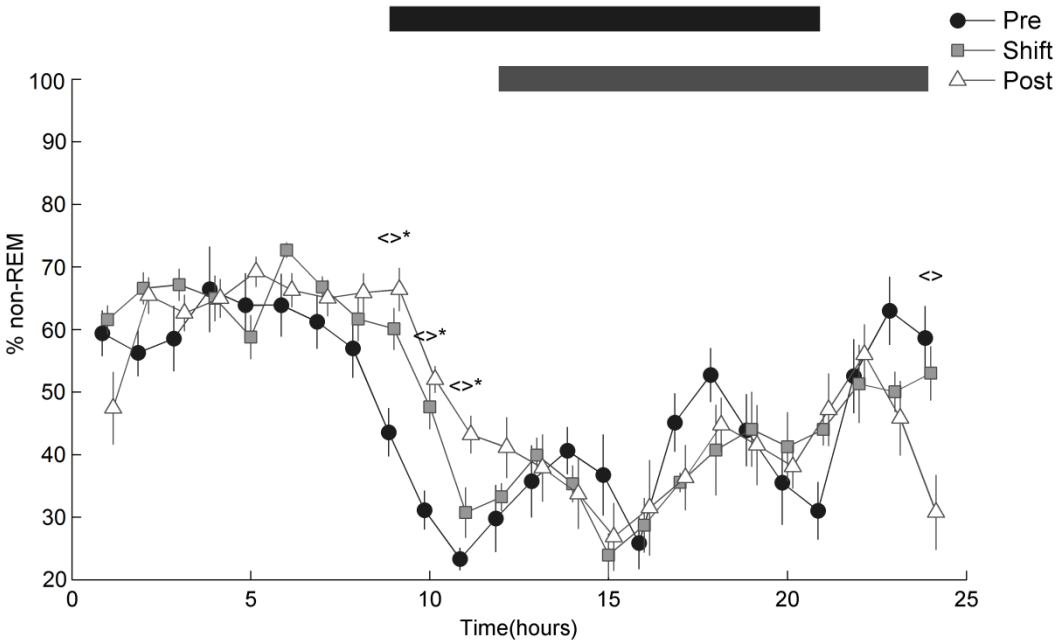
Pre
Shift
Post
% non-REM
Time(hours)
<>*
<>*
<>*
<>

4.4

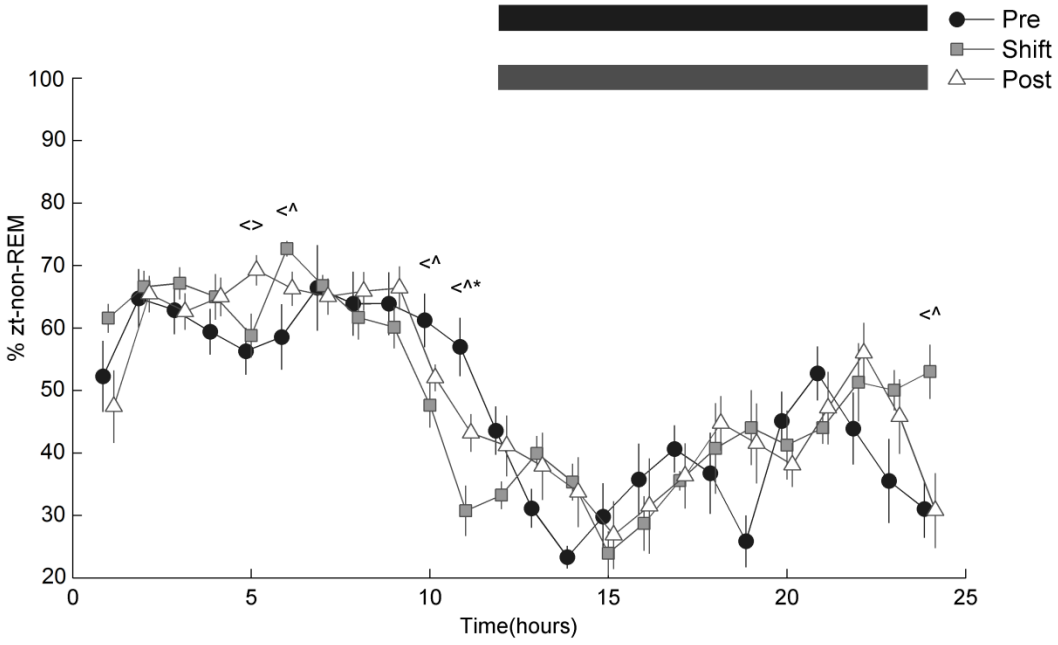
Pre
Shift
Post
% zt-non-REM
Time(hours)
<>
<^
<^
<^*
<^

4.5

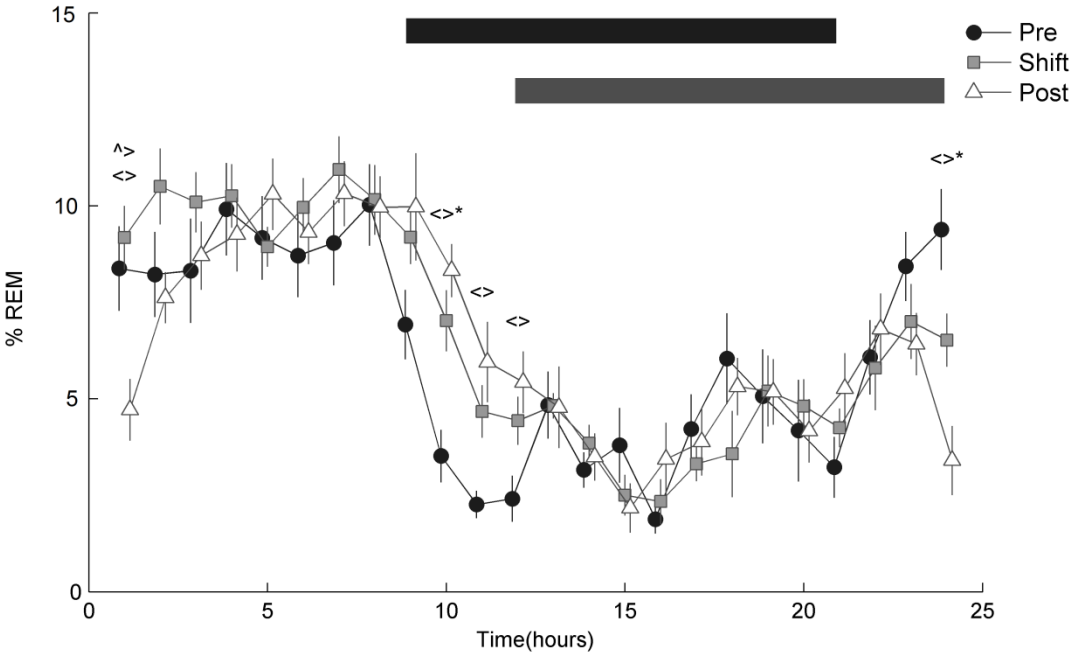
Pre
Shift
Post
% REM
Time(hours)
^>
<>
<>*
<>
<>
<>*
0
5
10
15
20
25

4.6

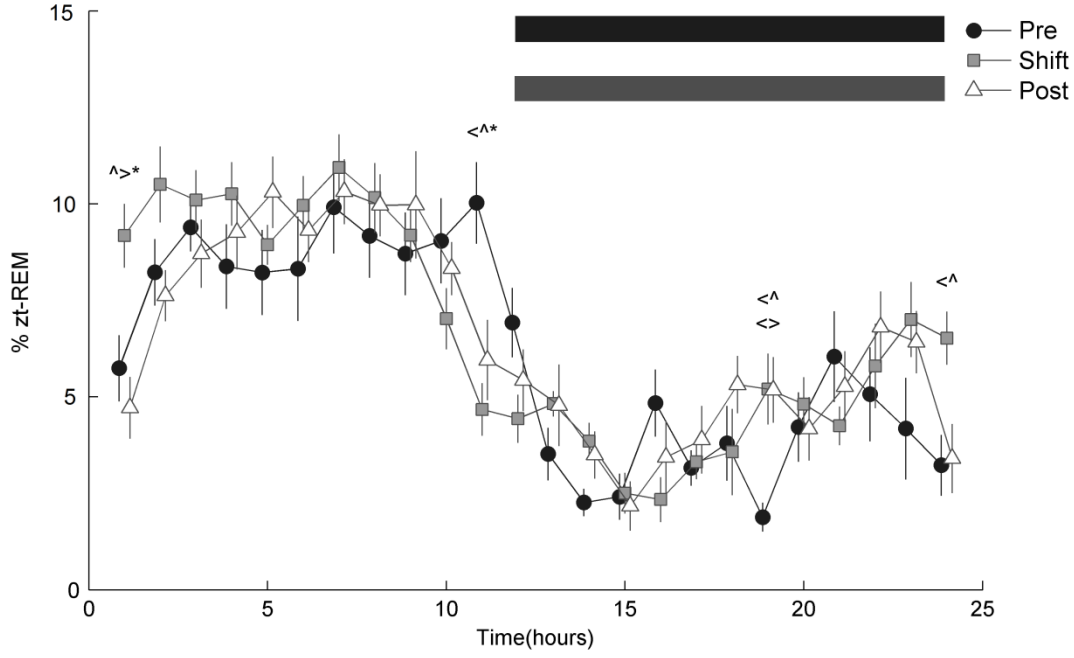
Pre
Shift
Post
% zt-REM
Time(hours)
^>*
<^*
<^
<>
<^
0
5
10
15
20
25

Figure 4. Distribution of hourly vigilance states (motionless, non-REM, and REM) in both **4.1, 4.3 and 4.5)** non-ZT and **4.2, 4.4 and 4.6)** ZT adjusted light/dark phases. Examined over a 24 hour period, plotted as a percentage of time per hour (plotted points shifted by +/- 0.15 hours for clarity). Hourly percent of vigilance states across rats (n = 8) is averaged and SEM (vertical error bars) for each hour across the 6 days of pre-entrainment, shift, and post-entrainment is plotted. Upper section contains black bars depicting dark phase of pre-entrainment and post-entrainment. Statistical significance testing ($P < 0.05$) was done using the KW and MC test across pre-entrainment to shift (< ^), shift to post-entrainment (^ >), and pre-entrainment to post-entrainment epochs (< >), p-values < 0.01 denoted by *.

3.4 No change to the quantity or density of LVS and k-complexes per day

KW tests ($P<0.05$) were used to compare the daily total duration, number, average length, and inter interval of LVS, and K-complex epochs across 6 days of pre-entrainment, shift, and post-entrainment. Figure 5.1, 5.2, 5.3, and 5.4 show no significant changes to the daily total duration, number, average length, and inter interval (respectively) of k-complex events when tested using a KW test ($P <0.05$) across pre-entrainment, shift, and post-entrainment epochs. Figure 5.5, 5.6, 5.7, and 5.8 shows no significant changes to the daily total duration, number, average length, and inter interval (respectively) of LVS events when tested using a KW test ($P <0.05$) across pre-entrainment, shift, and post-entrainment epochs. No significant change has been found to the daily mean density of k-complexes and LVS (Figure 6) when compared across pre-entrainment, shift and post-entrainment epochs, using a KW ($P <0.05$).

5.1

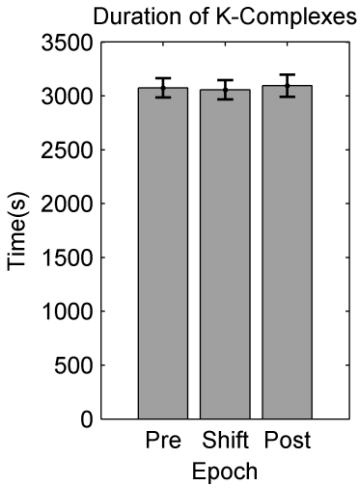

5.2

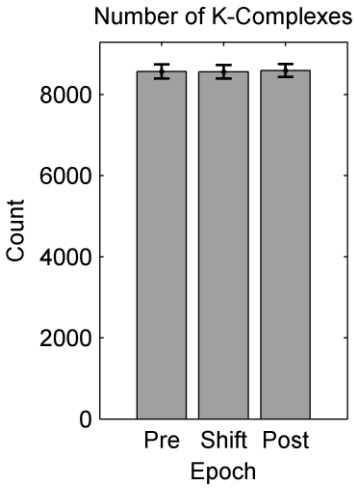

5.3

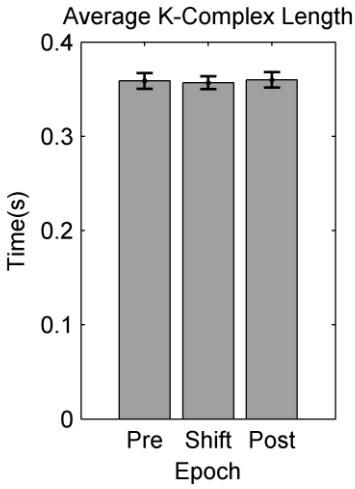

5.4

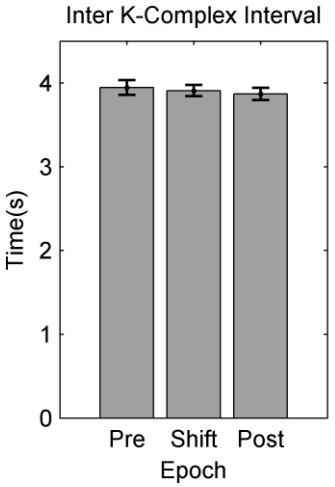

5.5

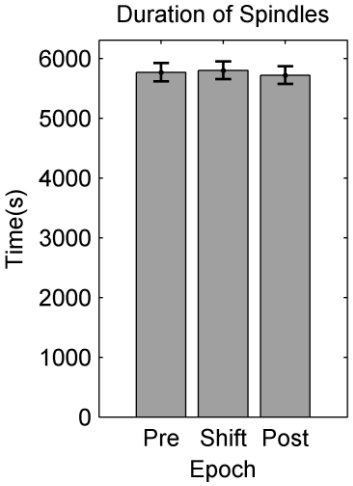

5.6

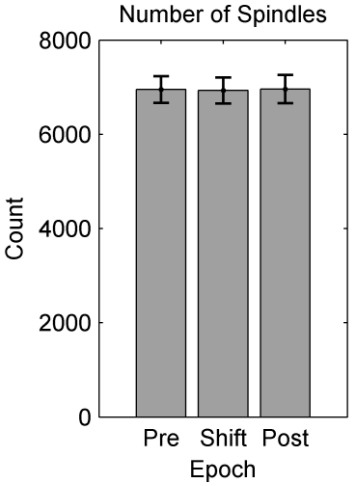

5.7

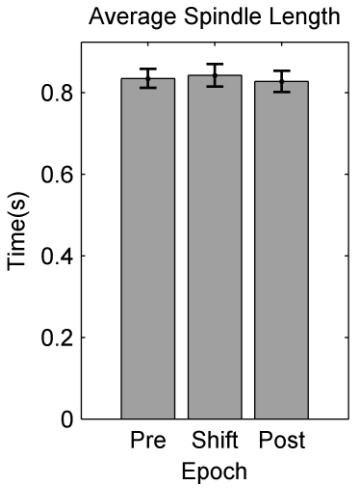

5.8

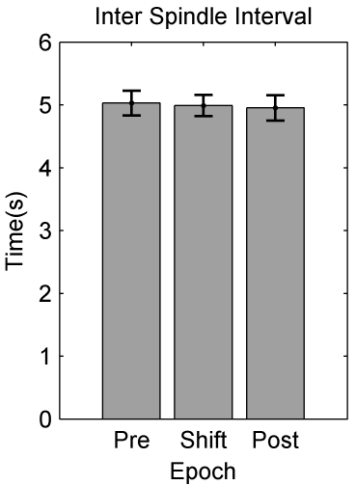

Figure 5. Mean daily quantities of k-complex and LVS (spindle) events across 6 days of pre-entrainment, shift, and post-entrainment epoch across rats. Vertical error bars represent SEM when comparing mean quantities amongst rats (n=7) of each day, across 6 days of pre-entrainment, shift and post-entrainment. Statistical significance was tested using a KW and MC test ($P < 0.05$). **5.1 , 5.2, 5.3, 5.4)** K-complex event analysis depicting the total duration, number of events, average length, and inter interval for. **5.5, 5.6, 5.7, 5.8)** LVS (spindle) event analysis depicting the total duration, number of events, average length, and inter interval.

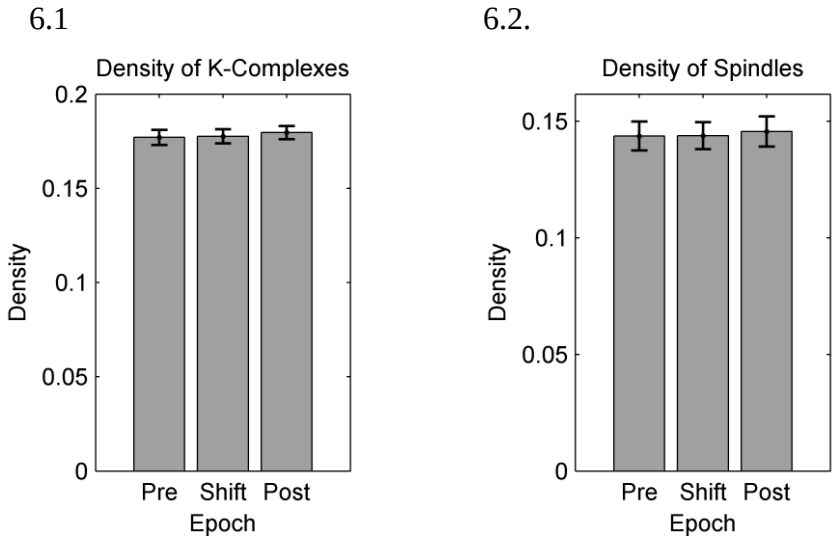

Figure 6. Mean daily density value of 6.1) k-complex and 6.2) LVS events across 6 days of pre-entrainment, shift, and post-entrainment epochs. Density is calculated as a ratio of the sum of LVS or k-complex event durations per hour to the sum of the duration of the motionless epochs per hour. Vertical error bars represent SEM when comparing mean values amongst rats (n=7) of each day across 6 days of pre-entrainment, shift and post-entrainment. Statistical significance was tested using a KW and MC test ($P < 0.05$).

3.5 Modification to the density distribution of LVS and k-complexes per hour

Examination of the hourly density distribution of k-complex and LVS events across pre-entrainment, shift, and post-entrainment epochs using a KW ($P<0.05$) and MC ($P<0.05$ and $P<0.01$) test, have shown significant changes when comparing the density of k-complexes across pre-entrainment to post-entrainment of hour 1 (KW $P<0.05$ and MC $P_{pre\text{-}post} < 0.01$, Figure 7.1), hours 8, 14, 23 (KW $P<0.05$ and MC $P_{pre\text{-}post} < 0.05$, Figure 7.1) and shift to post-entrainment hour 24 (KW $P<0.05$ and MC $P_{shift\text{-}post} < 0.01$, Figure 7.1.). ZT shifted values found a significant difference between the hourly density distributions of k-complex events in pre-entrainment to shift epochs on hour 7 (KW $P<0.05$ and MC $P_{pre\text{-}shift} < 0.05$, Figure 7.2). Significant changes to hourly LVS density distributions were also found on hour 5 between shift and post-entrainment (KW $P<0.05$ and MC $P_{shift\text{-}post} < 0.01$, Figure 7.3). When comparing ZT shifted LVS density distributions, a significant modification was found on hour 5 between shift to post-entrainment (KW $P<0.05$ and MC $P_{shift\text{-}post} < 0.01$, Figure 7.4) and pre-entrainment to post-entrainment (KW $P<0.05$ and MC $P_{pre\text{-}post} < 0.05$, Figure 7.4) epochs. These results indicate that hourly k-complex density distribution are significantly modified between pre-entrainment to post-entrainment epochs in non-ZT adjusted epochs (Figure 7.1), which are restored with a ZT shift (Figure 7.2). Hourly LVS density distributions are only modified on hour 5 in both non-ZT (Figure 7.3) and ZT adjustment conditions (Figure 7.4). Indicating the maintained post-entrainment light/dark cycle largely modified k-complex, but not LVS hourly distributions when compared to pre-entrainment.

7.1

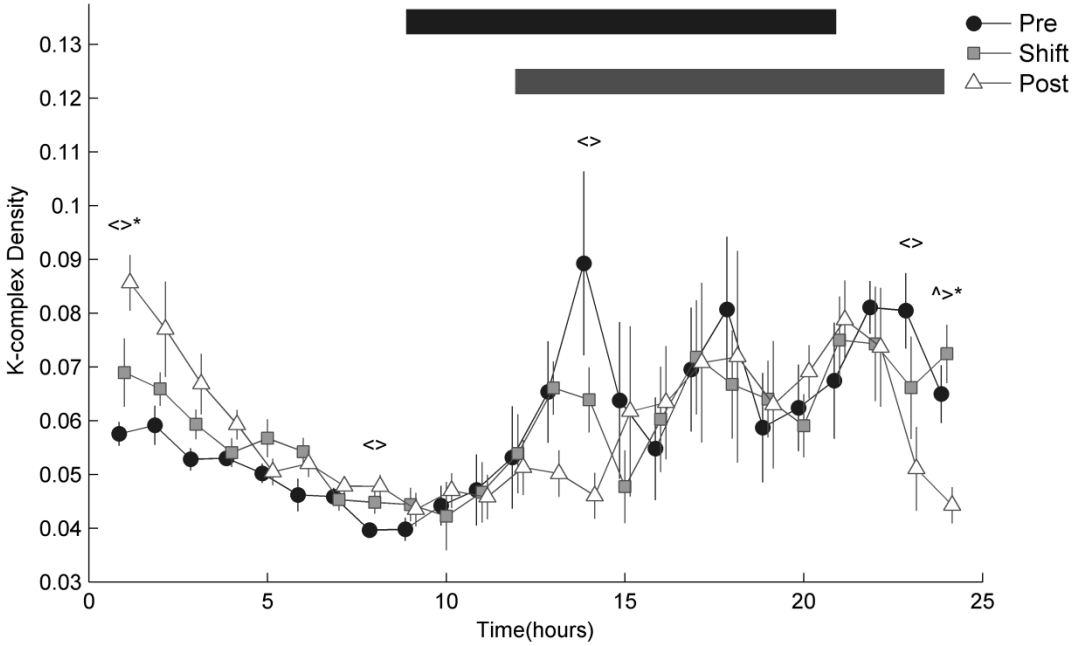
Pre
Shift
Post
K-complex Density
Time(hours)
<>*
<>
<>
^>*

7.2

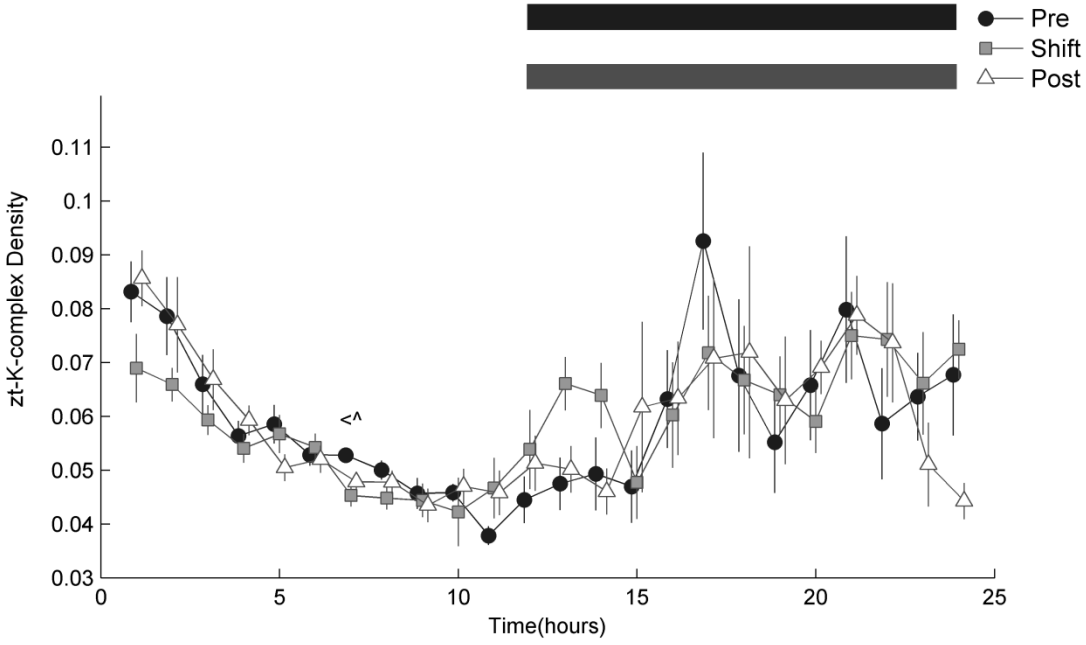
Pre
Shift
Post
zt-K-complex Density
Time(hours)
<^

7.3

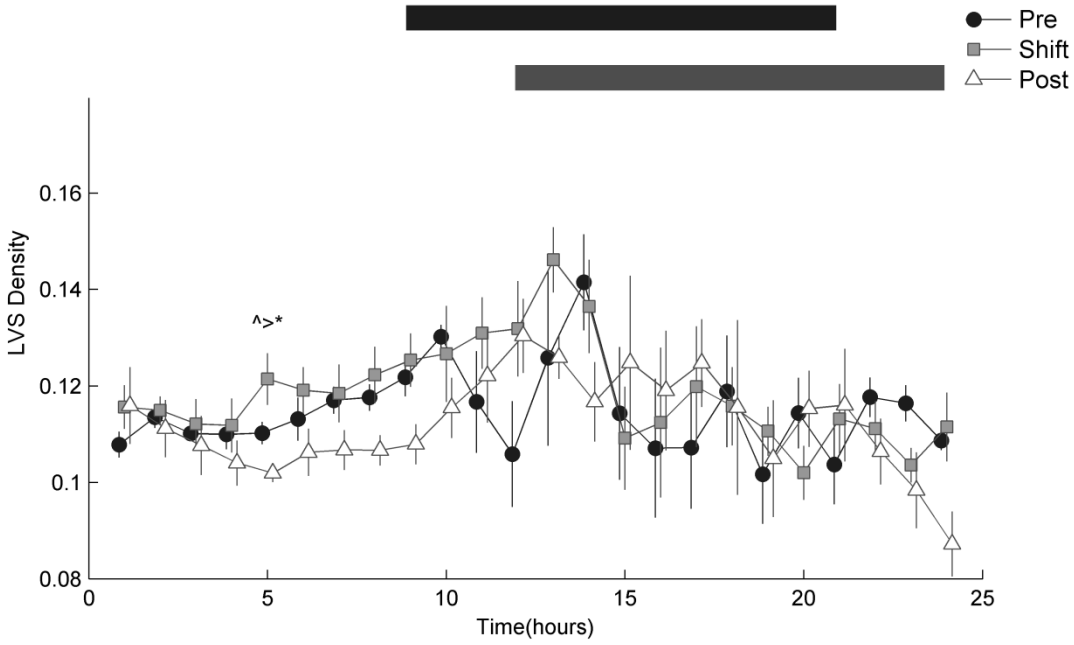
Pre
Shift
Post
LVS Density
0.16
0.14
0.12
0.1
0.08
^>*
0
5
10
15
20
25
Time(hours)

7.4

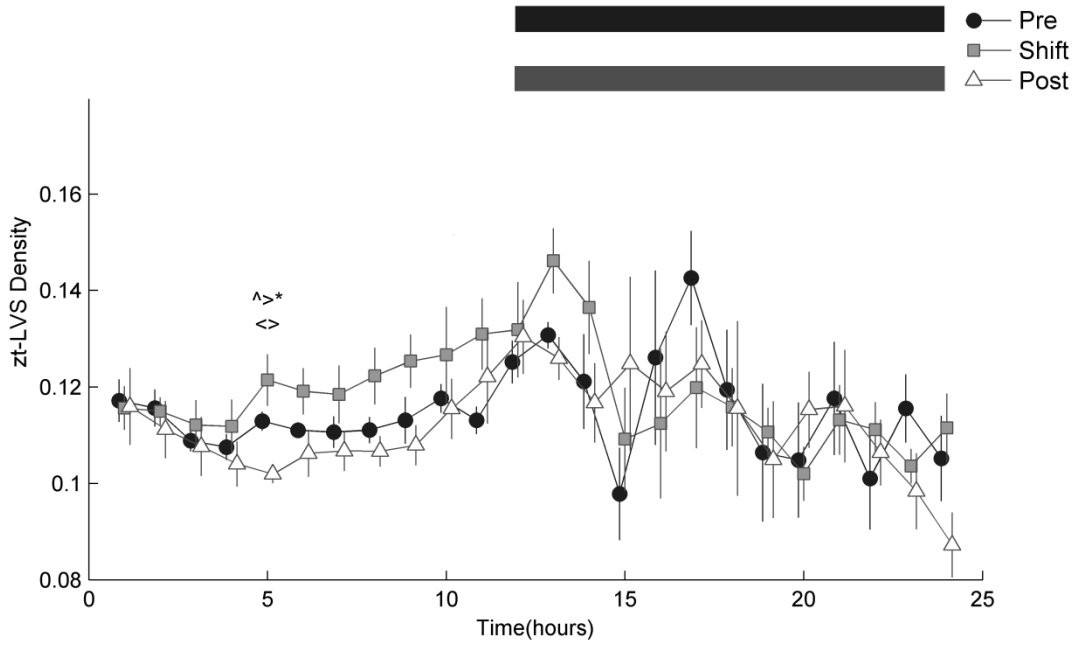
Pre
Shift
Post
zt-LVS Density
0.16
0.14
0.12
0.1
0.08
^>*
<>
0
5
10
15
20
25
Time(hours)

Figure 7. Density distribution of hourly k-complex and LVS examined over a 24 hour period in both **7.1 and 7.3)** non-ZT and **7.2 and 7.4)** ZT adjusted light/dark phases. Density is calculated as a ratio of the sum of LVS or k-complex event durations per hour to the sum of the duration of the motionless epochs per hour. Hourly density across rats (n = 7) is averaged and SEM (vertical error bars) for each hour across the 6 days of pre-entrainment, shift, and post-entrainment is plotted (plotted points shifted by +/- 0.15 hours for clarity). Upper section contains black bars depicting dark phase of pre-entrainment and post-entrainment. Statistical significance testing ($P < 0.05$) was done using a KW and MC test across pre-entrainment to shift (< ^), shift to post-entrainment (^ >), and pre-entrainment to post-entrainment epochs (< >), p-values < 0.01 denoted by *.

3.6 No change to the co-occurrence of k-complexes associated with LVS

No changes were found to the mean daily latency of k-complexes to LVS events between pre-entrainment, shift, and post-entrainment epochs ($P < 0.05$, Figure 8) when using a KW test. Distribution of peri-event time histograms (PETH) between k-complex (reference) and LVS (target) were tested using a KW test ($P<0.05$). PETH values for each individual day were averaged across 6 days of each pre-entrainment, shift, and post-entrainment group to create a mean PETH for each group. A KW test ($P<0.05$) was then performed across pre-entrainment, shift, and post-entrainment groups. No significant differences were found when comparing the PETH distributions of k-complex and spindle onsets (Figure 9) between pre-entrainment, shift, and post entrainment epochs when tested using a KW test ($p < 0.05$).

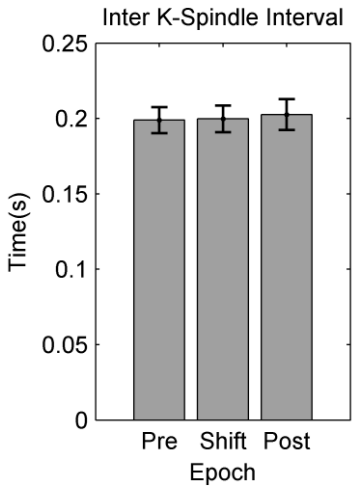

Figure 8. Mean daily inter intervals of k-complexes (reference) and LVS (target) events across 6 days of pre-entrainment, shift, and post-entrainment. Vertical error bars represent SEM when comparing the mean values amongst rats (n=7) of each day across 6 days of pre-entrainment, shift and post-entrainment across rats. Statistical significance was tested using a KW and MC test ($P < 0.05$) between pre-entrainment, shift and post-entrainment epochs.

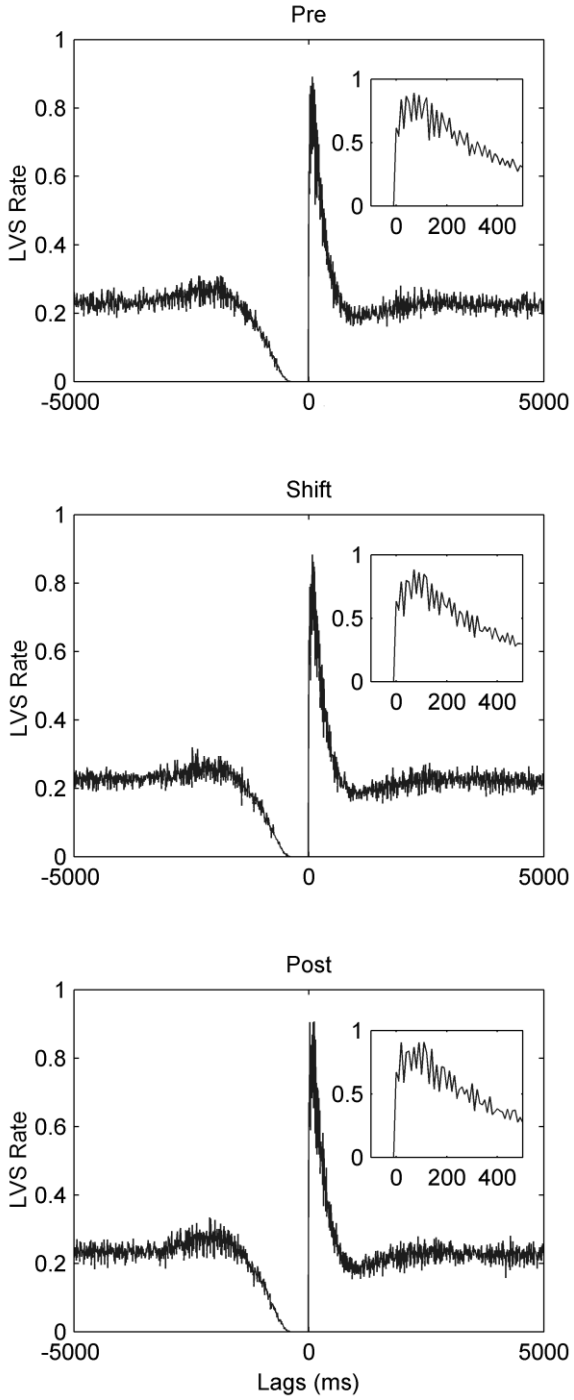

Figure 9. Cross-correlation of K-complex to LVS events normalized such that it represents a PETH depicting relative time of occurrence centered at a reference k-complex (timestamp taken from the center of k-complex start and end time) and target

LVS (timestamp taken from the start time of a LVS). The number of LVS observed in each bin centered on k-complex events is counted and divided by the bin width (10ms) and the total number of k-complexes. This gives the average rate of LVS occurrences in each of these bins when a k-complex event is observed. 500 bins have been shown on each side of time zero. Measurement taken across rats (n = 7) of 6 days of pre-entrainment, shift and post-entrainment.

4. Discussion

In the present study, analyses performed on continuous LFP recordings suggest that the hourly distribution of delta power epochs (Figure 2) events have not been modified by an acute circadian dark phase advance across pre-entrainment, shift, and post-entrainment. The daily percent of time, number, and average length of motionless, non-REM, and REM vigilance states (Figure 3) have not been modified by an acute circadian shift when compared across pre-entrainment, shift, and post-entrainment epochs. Indicating vigilance state quantity is strongly maintained across the current acute circadian shifting paradigm. Functionally, this provides evidence that a change in motionless, non-REM, and REM quantity does not describe the disruption of spatial memory retention observed in an acute circadian shift. Similarly, hourly vigilance distributions were not largely effected during the acute shift, when comparing non-ZT adjusted pre-entrainment to shift and shift to post entrainment (Figure 4.1, 4.3, and 4.5).

Contrastingly, the current acute circadian shifting paradigm selectively modifies the hourly distribution of motionless, non-REM and REM states (Figure 4.1, 4.3, and 4.5) predominantly when comparing pre-entrainment to post-entrainment epochs, which can be restored using a ZT adjustment (Figure 4.2, 4.4, and 4.6). These results support the proposal that a mechanism of spatial memory retention (but not acquisition) is impaired in post entrainment, as we have found that post-entrainment hourly vigilance state distributions differ significantly from pre-entrainment, but not shifting epochs. No other reports (Frankland and Bontempi, 2005;Cirelli, 2009;Diekelmann and Born, 2010) have suggested that an adjustment in maintained hourly sleep structure are implicated in the spatial memory retention impairments observed in an acute shift. Suggesting it is

unlikely that the maintained, but adjusted hourly distribution of vigilance states is responsible for the spatial memory retention deficits observed in an acute circadian shift. As a result of this we investigated further into the manipulation of an acute circadian shift on sleep based events.

Critically, the current experiment is also able to conduct an investigation of k-complex, and LVS events. The total duration, number, average length and inter interval of k-complex and LVS events per day are also robust against an acute circadian shift (Figure 5). This suggests that an acute circadian shift does not modify the quantity of k-complexes and LVS events, again suggesting that sleep quantity is strongly maintained in an acute circadian shifting paradigm. Functionally, this provides evidence that a change in sleep event quantity does not describe the disruption of spatial memory retention observed in an acute circadian shift. Furthermore, the daily density of k-complex and LVS events is not modified (Figure 6) by an acute circadian shift. LVS hourly density distributions only showed modification to hour 5 in both non-ZT (Figure 7.3) and ZT adjusted (Figure 7.4) conditions, which is likely not of any functional significance due to a single change only on hour 5. Additionally, k-complex density distributions were not largely effected during the acute shift, when comparing non-ZT adjusted pre-entrainment to shift and shift to post-entrainment (Figure 7.1). Suggesting that both k-complex and LVS daily quantity is maintained during the shifting epoch of an acute circadian shift.

In contrast, hourly k-complex density distribution are significantly modified primarily between pre-entrainment to post-entrainment epochs in non-ZT adjusted epochs (Figure 7.1), which are largely restored with a ZT shift (Figure 7.2). K-complex density has been positively correlated with stored-trace reactivation (Johnson et al., 2010),

indicating this modification is functionally relevant. Adjustment of maintained k-complex hourly density distributions across pre-entrainment to post-entrainment supports the finding that an acute circadian shift disrupts memory retention in the post-entrainment epoch, but not acquisition during the shifting epoch.

The proceeding discussion will further highlight the functional significance of strongly maintained daily sleep quantities. Furthermore, maintained hourly vigilance states and k-complexes distributions adjusted across pre-entrainment to post-entrainment epochs will be discussed. Additionally, we will consider the relationship between sleep based events, adjustments of their distributions, and their relationship to spatial memory retention.

4.1 No change to hourly delta power distribution

Delta power has been implicated as a key mechanism of homeostatic regulation (Borbely and Neuhaus, 1979). While an acute circadian shift did not modify the total quantity of sleep based vigilance states per day, it was also important to investigate possible changes to mechanisms regulating homeostasis of the rat in this paradigm. Multiple studies have been aimed at investigating prior waking activity and its effect on homeostatic mechanisms regulating sleep (Tobler and Borbely, 1986;Dijk et al., 1987;Lancel et al., 1991;Deboer and Tobler, 2003), but the effects of acute circadian disruption on homeostatic mechanisms are not known. The present study indicates that an acute circadian shift did not modify the hourly distribution of delta power in both non-ZT (Figure 2.1) and ZT (Figure 2.2) across pre-entrainment, shift, and post-entrainment epochs. Suggesting that sleep debt has not accumulated as a result of our acute circadian

shift paradigm and hourly delta amplitude is robust against an acute circadian dark phase advance.

4.2 No change to daily quantity of motionless, non-REM, and REM; hourly distribution maintained, but adjusted

The present data have shown that the daily total percent of motionless, REM, and non-REM sleep quantities are robust against an acute circadian shift, when compared across pre-entrainment, shift and post-entrainment epochs (Figure 3). Previously, Loh et al. (2010) have investigated changes to motionless, REM and non-REM vigilance states in a one day dark phase advance paradigm. The one day dark phase advance used by Loh et al. (2010) has not shown changes to the total daily amount of these vigilance states, when compared across one day of pre-entrainment, shift, and post-entrainment (three days total). This also supports the finding that the circadian and homeostatic events regulated by the daily quantity of sleep based vigilance states are also maintained in a dark phase advance paradigm. Loh et al. (2010) have not found changes to the hourly distribution of motionless vigilance states across a one day phase advance, which were present in a one day phase delay. In contrast, we have found significant changes to the hourly distribution of motionless, non-REM, and REM epoch lengths when compared across pre-entrainment, shift, and post-entrainment epochs (Figure 4) in a six day phase advance. These differences have been found predominantly in pre-entrainment to post-entrainment epochs. In order to clarify when post-entrainment hourly distributions become significantly difference from pre-entrainment, the amount of time spent in motionless, non-REM, and REM were compared between each day by looking at each day's hourly distribution and computing a Pearson correlation coefficient between all pairs of days (Figure 10).

We have found a correlation decrease in hourly distributions of motionless, non-REM and REM sleep during the three hour phase advance, when comparing pre-entrainment to shift epochs (Figure 10.1, section i), which is continued in pre-entrainment to post-entrainment (Figure 10.1, section iii). The decrease in correlation is observable by the increase in non-significant correlation values (white squares, in Figure 10) and in the decreased correlation values when comparing pre-entrainment to post-entrainment described in Table 1. The decrease in correlation visibly begins on day 10 (Figure 10.1, section i, x-axis reference) of the phase shifting paradigm in motionless, non-REM and REM sleep, at which point there is a complete phase reversal of the light/dark light schedule (Table 1). This finding suggests that a shift in motionless, non-REM and REM vigilance states occurs the on the 10^{th} day, whereby a light/dark reversal is implemented. A reduced correlation between pre-entrainment to shifting epochs also leads to an increased correlation between shifting to post-entrainment epochs on day 9 (Figure 10.1, section ii, y-axis reference) in motionless, non-REM and REM vigilance states. An enhanced correlation of shifting to post-entrainment epochs indicates that the change observed during shifting epochs is advancing the distribution of shifting epochs towards post-entrainment epochs. Interestingly, when a ZT shift is applied (increasing each pre-entrainment hourly distribution by 3 hours) pre-entrainment to post entrainment day by day correlation values increase (Figure 10.2, section iii, Table 2). The observed increase in correlation between pre-entrainment to post-entrainment in ZT suggests that the rats have preserved pre-entrainment distributions, but have adjusted their hourly vigilance state distributions by three hours in post-entrainment. Subsequently this adjustment aligns the three hour phase delay maintained in post-entrainment with pre-entrainment

light/dark cycle. We can infer that distributions of vigilance states between pre-entrainment and post-entrainment are maintained, but advanced by three hours.

	non-ZT			ZT		
	Pre-Shift	Shift-Post	Pre-Post	Pre-Shift	Shift-Post	Pre-Post
Delta	0.75	0.61	0.28	0.60	0.61	0.78
Motionless	0.82	0.86	0.61	0.70	0.86	0.85
Non-REM	0.80	0.86	0.60	0.69	0.86	0.85
REM	0.84	0.84	0.62	0.71	0.84	0.83
K Density	0.74	0.60	0.34	0.72	0.60	0.76
LVS Density	0.54	0.46	0.12	0.52	0.46	0.53

Table 2. Hourly distribution correlation comparison across pre-entrainment to shift, shift to post-entrainment and pre-entrainment to post-entrainment taken from distributions in Figure 2, Figure 4 and Figure 7 matched to ZT shifted values taken from supplemental Figure 1. Correlation values were measured using a Pearson's linear correlation coefficient (all p-values presented are < 0.05). Note increase in pre-post values in ZT shift.

10.1

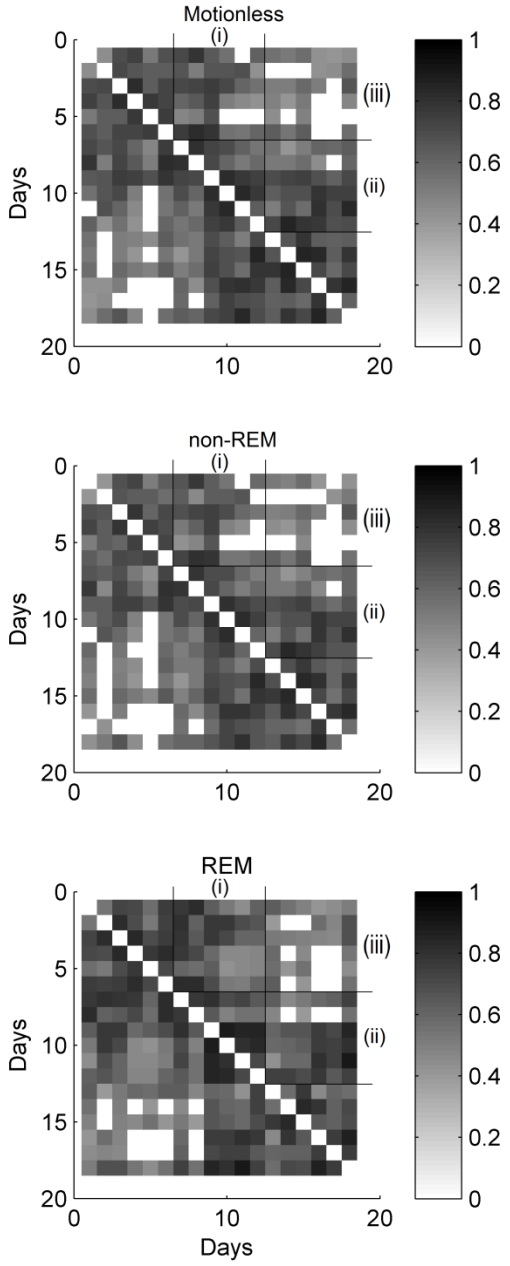
Motionless
non-REM
REM
(i)
(ii)
(iii)
Days
0
5
10
15
20
0.2
0.4
0.6
0.8
1

10.2

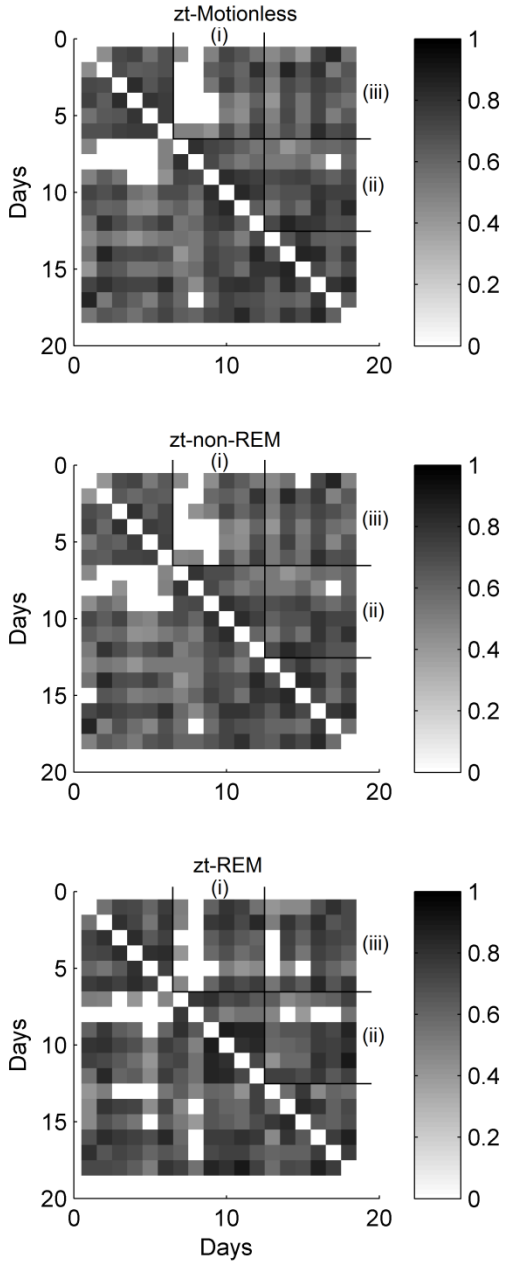
zt-Motionless
zt-non-REM
zt-REM
(i)
(ii)
(iii)
Days
0
5
10
15
20
0.2
0.4
0.6
0.8
1

Figure 10. Day by day vigilance state cross correlation values across rats (n = 8) between days, calculated for hourly distributions ($P < 0.05$) of motionless, non-REM (SWS), and REM vigilance states for **10.1)** non-ZT and **10.2)** ZT 3 hour adjustment. Correlation values are mirrored across the diagonal. Colour map indicates level of correlation, non-significant ($P > 0.05$) days have been set to 0 (marked white). Areas marking correlations between pre-entrainment to shift (i), shift to post-entrainment (ii), and pre-entrainment to post-entrainment (iii) have been outlined. Note decrease in correlation between pre-entrainment and shift on day 7 in ZT adjusted area (i) due to ZT adjustment. Area iii of Figure 10.1 shows a reduced day-day correlation when comparing pre-entrainment to post-entrainment, which is increased with ZT shift (Figure 10.2, section iii).

4.3 No change to daily quantity of k-complexes, and spindles; hourly distribution maintained, but adjusted

The daily total duration, number, inter-interval (Figure 5), and density (Figure 6) of K-complex and LVS events were not found to be modified by an acute circadian shift when compared across pre-entrainment, shift and post-entrainment epochs. This indicates that these quantities of k-complex and LVS activity are robust against an acute circadian shift. In the present study, we have found modifications to the hourly distribution of k-complex event density, which predominantly occur between pre-entrainment to post-entrainment epochs (Figure 7.1) and modulation to the density of LVS on hour 5 (Figure 7.3). When pre-entrainment epochs are shifted to ZT (Figure 7.2 and Figure 7.4), we observe less modification to the hourly k-complex distribution and a slightly larger effect on hour 5 of the hourly LVS distribution, which is likely of no functional significance. From this we can conclude that the hourly distribution of k-

complex events are modified when comparing pre-entrainment to post-entrainment epochs, which is restored with a ZT alignment (Table 2 and Figure 7.2). As previously mentioned, hourly distribution modification between pre-entrainment and post-entrainment, which are restored using a ZT adjustment was also observed in hourly motionless, non-REM and REM ZT adjusted values (Figure 10, Table 2, Figure 4.2, Figure 4.4, and Figure 4.6).

We have also shown that LVS density both daily (Figure 6.2) and hourly density distributions is maintained in non-ZT (Figure 7.3) and ZT manipulations (Figure 7.4), with only hour 5 showing variation in hourly density distributions. The resistance to hourly distribution modification displayed by LVS is thought-provoking and warrants future investigation. As mentioned previously, cortical spindling has been widely implemented as a mechanism used to facilitate memory consolidation (Gais and Born, 2004;Eschenko et al., 2006). The strong maintenance of both the daily quantities and LVS hourly distributions against an acute circadian phase advance may be in response to preserving the aforementioned consolidation mechanism. To the knowledge of these authors, no other reports have been made on the effects of acute circadian disruption and cortical spindle activity. Further work involving modifications to the amount and timing of circadian shifting and LVS activity will provide more insight into the functional role of cortical spindling and sleep.

Furthermore, we have looked at the relationship between k-complex and LVS events. In general, k-complex detection occurs with an associated spindle, but this co-occurrence is not essential (Amzica and Steriade, 2002). Our analyses have not detected modification to the mean distance between k-complexes and LVS (Figure 8) or to the

PETH distribution between k-complexes associated with LVS across pre-entrainment, shift and post entrainment epochs (Figure 9). The relationship between k-complex and spindling events is strongly preserved across an acute photic phase advance, suggesting that the association between these two events plays a necessary functional role in sleep.

4.4 Interactions between sharp wave ripples (SWR), LVS, and k-complexes

Our findings indicate that there is not a significant change to the quantity or distribution (hourly distributions preserved, but adjusted with post-entrainment) of the sleep based events we have investigated, it is possible that modifications are being made to the relationship between SWR, LVS and k-complex events. These alterations may be responsible for the deficit observed by an acute circadian shift in retention, but not acquisition of a spatial memory. Hippocampal sharp waves can be described as, lasting 50-150ms and are coupled with faster oscillatory discharges producing a SWR at a frequency near 200Hz (Buzsaki, 1986;Chrobak and Buzsaki, 1998). Hippocampal replay strength peaks during SWRs (Peyrache et al., 2009) and selective elimination of SWRs during slow wave sleep has been shown to impair post-sleep hippocampal task dependent performance (Girardeau et al., 2009;Ego-Stengel and Wilson, 2010). Co-occurrence between SWR and spindle activity has been demonstrated by multiple research groups (Siapas and Wilson, 1998;Molle et al., 2006). As well, Battaglia et al. (2004) have shown that SWR activity coincides with cortical delta oscillations. Further work has shown that cellular firing sequences evoked by waking activity both in cortical and hippocampal regions are replayed in an organized pattern during subsequent sleep sessions (Sirota et al., 2003;Ji and Wilson, 2007). The occurrence of these events lends to the theory that coordinated hippocampal and cortical replay increasingly strengthens

cortical to cortical interactions, allowing new memories to become independent of the hippocampus (Frankland and Bontempi, 2005). Although the relationship of these non-REM sleep based events to learning and memory has been extensively investigated, their connection to the spatial memory retention deficits observed in acute circadian disruption is not known. Acute circadian disruption may reduce the number of hippocampal SWR events. Furthermore, if hippocampal SWR activity is shown to be stable across an acute circadian shift, interactions between hippocampal SWR and cortical LVS may be disrupted. This hippocampal and cortical disruption may also occur in relation to the maintained, but adjusted distribution of hourly sleep events.

4.5 Effect of a learning experience

Currently, our experimental protocol has not implemented a learning paradigm (i.e. rats were in a steady state). Extending the current investigation by observing sleep hourly distribution adjustments in parallel with spatial memory retention on a MWM would further describe a relationship between hourly sleep structure and spatial memory retention. By implementing this experimental protocol it would be possible to observe a correlation between MWM spatial memory retention and sleep structure adjustments. Furthermore, sleep events shown to be modified by learning experiences may not be affected by an acute circadian shift without implementing a learning paradigm.

Spindling activity has been shown to be highly dependent on a learning experience (Gais and Born, 2004;Eschenko et al., 2006) and SWR activity is correlated with performance on a spatial learning task (Girardeau et al., 2009;Ego-Stengel and Wilson, 2010). These findings indicate that both spindling and SWR activity is modified

by a learning paradigm. We have not observed changes to the quantity of LVS and k-complex events (Figure 5) or relationship of LVS to k-complexes (Figure 8 and 9). Furthermore, we only see one modifications between hourly LVS density distributions in hour 5 of non-ZT adjusted time.

In this experiment the observed lack of modification to LVS events may result from the absence of a learning experience. Additional examination into the effect of circadian modulation on k-complex and spindling events in relation to a learning experience is required. Furthermore, this protocol can be expanded to include neuronal unit recordings. Unit recordings are capable of recording from single neurons in a freely behaving animal and would allow for the investigation of spatial mapping on a cellular level in hippocampal place cells.

Prior investigation has shown hippocampal place cells that fire together during a task have a higher probability of firing during a subsequent sleep (Wilson and McNaughton, 1994). In this case, modification to hippocampal firing patterns during a post-task sleep can be accounted for by a task dependent learning experience. Currently, this experiment did not include unit recordings, so it was not possible to observe changes to hippocampal or cortical unit activity in relation to an acute circadian shift. Further investigation with unit recordings under circadian disruption, coupled with a spatial learning paradigm (for example a MWM protocol) would provide more insight into the role circadian cycles play in a spatial learning.

4.6 System, synaptic, and cellular consolidation

The current investigation was focused on mechanisms believed to be involved in a standard two stage model of memory consolidation. Whereby, patterns learned both by a hippocampal fast learner and neocortical slow learner are replayed during sleep, creating both a temporary and long-term memory store respectively. Slow oscillations group neuronal activity into down and up states allowing for periods of neuronal silence and enhanced neuronal activity respectively (Molle and Born, 2011). Cortical LVS and hippocampal SWR activity commonly occur in relation to these up-down state transitions, which are hypothesized to play a critical role in systems consolidation in the standard two stage model of memory consolidation. In Devan et al. (2001) memory acquisition of a platform location was not impaired, demonstrating that learning had taken place. A deficit was observed when the rats were again tested 7 or 17 days later, showing special memory retention impairment in acutely shifted groups. This finding illustrates a probable deficit to the systems level of consolidation, based on the finding that long term retrieval and/or storage of the platform location was impaired, while maintaining initial memory encoding. In the current study we have found a higher correlation in ZT adjusted k-complex density distributions (Table 2 and Figure 7.2), when comparing pre-entrainment with post-entrainment epochs. It is possible that while this advance occurs a miss-alignment between spindling and SWR is also transpiring. As previously mentioned, a continued inspection of the effects of circadian disruption on the co-occurrence of k-complexes, LVS and SWR would further illuminate this relationship. In correspondence with the standard two stage model of systems consolidation, a model of long term potentiation (LTP) can also be used to describe memory consolidation processes.

LTP can be described a lasting enhancement of connection strength between two neurons. LTP has been shown to be enhanced with a learning paradigm (Rioult-Pedotti et al., 2000). Tononi and Cirelli (2003) hypothesize that waking behaviour is tied to synaptic potentiation, while slow-wave activity is associated with synaptic long term depression (LTD). Furthermore, during slow-wave activity co-ordinated SWR and LVS activity is suggested to maintain synaptic connections, which have been modulated during waking behaviour. It is also possible that the changes observed in the Devan et al. (2001) study may be due to modifications of LTP or LTD mechanisms responsible for memory maintenance. Furthermore, cellular processes additionally describe mechanisms involved in long-term memory formation.

cAMP-responsive element-binding protein (CREB) has been shown to be necessary for the formation of long term memories (Kandel, 2001). dCREB2 (drosophila homolog of CREB) mutants have been shown to dampen the oscillation of period (PER) clock genes (Belvin et al., 1999), which are necessary for circadian molecular clock function. Additionally, PER has been shown to play a key role in long-term memory formation (Sakai et al., 2004). PER levels are shown to be reduced by circadian disruption, while still maintaining daily quantities of waking, non-REM, and REM sleep (Castanon-Cervantes et al., 2010). Similarly, we have found that daily quantities of sleep are maintained across an acute circadian shift, suggesting the disruption of cAMP and PER may play a large role in the disruption of memory retention observed in the currently explored acute circadian dark phase advance. Possibly, cAMP and PER activation may be modified with the adjustment of maintained hourly sleep distributions. We would predict that this would result in the observed memory retention deficits with

maintain daily sleep quantities in the currently investigated acute circadian disruption paradigm. Investigation into the timing of cAMP and PER modification, in relation to distribution phase adjustments of vigilance states and k-complexes would further highlight how cAMP and PER are altered by circadian disruption.

4.7 Conclusions

The results of this study indicate that an acute circadian dark phase advance strongly maintains daily quantities of sleep. Suggesting sleep quantity is maintained during the currently investigated acute circadian shift. Sleep hourly distributions show little modification during the shifting epoch, when comparing pre-entrainment to shift and shift to post-entrainment. Contrastingly, significant effects are observed when comparing pre-entrainment to post-entrainment hourly sleep distribution epochs. Observed modifications to hourly distributions are markedly reduced when pre-entrainment distributions are aligned using ZT with post-entrainment hourly distributions, suggesting that hourly pre-entrainment sleep distributions are maintained but adjusted in phase with post-entrainment. Maintained hourly sleep distributions adjusted across pre-entrainment to post-entrainment clearly illustrate modification to sleep structure, supporting previous findings of disrupted spatial memory retention during post-entrainment. These modifications are not primarily observable during shifting epochs, corroborating previous evidence of conserved spatial memory acquisition during shifting epochs. In summary, highlighting maintained sleep structure predominantly adjusted across pre-entrainment and post-entrainment, but not during shifting epochs provides a critical first step to understanding the mechanisms responsible for memory retention impairments observed previously in an acute circadian shift.

5. References

Amzica, F., and Steriade, M. (2002). The functional significance of K-complexes. *Sleep Med Rev* 6**,** 139-149. doi: S1087079201901819 [pii].

Antoniadis, E.A., Ko, C.H., Ralph, M.R., and Mcdonald, R.J. (2000). Circadian rhythms, aging and memory. *Behav Brain Res* 114**,** 221-233. doi: S0166432800002904 [pii].

Barrett, T.R., and Ekstrand, B.R. (1972). Effect of sleep on memory. 3. Controlling for time-of-day effects. *J Exp Psychol* 96**,** 321-327.

Battaglia, F.P., Sutherland, G.R., and Mcnaughton, B.L. (2004). Hippocampal sharp wave bursts coincide with neocortical "up-state" transitions. *Learn Mem* 11**,** 697-704. doi: 10.1101/lm.73504.

Beelen, T. EDF Browser.

Belvin, M.P., Zhou, H., and Yin, J.C. (1999). The Drosophila dCREB2 gene affects the circadian clock. *Neuron* 22**,** 777-787.

Bertram, E.H., Williamson, J.M., Cornett, J.F., Spradlin, S., and Chen, Z.F. (1997). Design and construction of a long-term continuous video-EEG monitoring unit for simultaneous recording of multiple small animals. *Brain Res Brain Res Protoc* 2**,** 85-97.

Borbely, A.A., and Neuhaus, H.U. (1979). Sleep-Deprivation - Effects on Sleep and Eeg in the Rat. *Journal of Comparative Physiology* 133**,** 71-87.

Buzsaki, G. (1986). Hippocampal sharp waves: their origin and significance. *Brain Res* 398**,** 242-252. doi: 0006-8993(86)91483-6 [pii].

Castanon-Cervantes, O., Wu, M., Ehlen, J.C., Paul, K., Gamble, K.L., Johnson, R.L., Besing, R.C., Menaker, M., Gewirtz, A.T., and Davidson, A.J. (2010). Dysregulation of inflammatory responses by chronic circadian disruption. *J Immunol* 185**,** 5796-5805. doi: 10.4049/jimmunol.1001026.

Cho, K., Ennaceur, A., Cole, J.C., and Suh, C.K. (2000). Chronic jet lag produces cognitive deficits. *J Neurosci* 20**,** RC66.

Chrobak, J.J., and Buzsaki, G. (1998). Operational dynamics in the hippocampal-entorhinal axis. *Neurosci Biobehav Rev* 22**,** 303-310. doi: S0149-7634(97)00016-X [pii].

Cirelli, C. (2009). The genetic and molecular regulation of sleep: from fruit flies to humans. *Nat Rev Neurosci* 10**,** 549-560. doi: 10.1038/nrn2683.

Craig, L.A., and Mcdonald, R.J. (2008). Chronic disruption of circadian rhythms impairs hippocampal memory in the rat. *Brain Res Bull* 76**,** 141-151. doi: 10.1016/j.brainresbull.2008.02.013.

Deboer, T., and Tobler, I. (2003). Sleep regulation in the Djungarian hamster: comparison of the dynamics leading to the slow-wave activity increase after sleep deprivation and daily torpor. *Sleep* 26**,** 567-572.

Devan, B.D., Goad, E.H., Petri, H.L., Antoniadis, E.A., Hong, N.S., Ko, C.H., Leblanc, L., Lebovic, S.S., Lo, Q., Ralph, M.R., and Mcdonald, R.J. (2001). Circadian phase-shifted rats show normal acquisition but impaired long-term retention of place

information in the water task. *Neurobiol Learn Mem* 75**,** 51-62. doi: 10.1006/nlme.1999.3957.

Diekelmann, S., and Born, J. (2010). The memory function of sleep. *Nat Rev Neurosci* 11**,** 114-126. doi: 10.1038/nrn2762.

Dijk, D.J., Beersma, D.G., and Daan, S. (1987). EEG power density during nap sleep: reflection of an hourglass measuring the duration of prior wakefulness. *J Biol Rhythms* 2**,** 207-219.

Ego-Stengel, V., and Wilson, M.A. (2010). Disruption of ripple-associated hippocampal activity during rest impairs spatial learning in the rat. *Hippocampus* 20**,** 1-10. doi: 10.1002/hipo.20707.

Eschenko, O., Molle, M., Born, J., and Sara, S.J. (2006). Elevated sleep spindle density after learning or after retrieval in rats. *J Neurosci* 26**,** 12914-12920. doi: 10.1523/JNEUROSCI.3175-06.2006.

Fekete, M., Van Ree, J.M., Niesink, R.J., and De Wied, D. (1985). Disrupting circadian rhythms in rats induces retrograde amnesia. *Physiol Behav* 34**,** 883-887.

Frankland, P.W., and Bontempi, B. (2005). The organization of recent and remote memories. *Nat Rev Neurosci* 6**,** 119-130. doi: 10.1038/nrn1607.

Gais, S., and Born, J. (2004). Declarative memory consolidation: mechanisms acting during human sleep. *Learn Mem* 11**,** 679-685. doi: 10.1101/lm.80504.

Girardeau, G., Benchenane, K., Wiener, S.I., Buzsaki, G., and Zugaro, M.B. (2009). Selective suppression of hippocampal ripples impairs spatial memory. *Nat Neurosci* 12**,** 1222-1223. doi: 10.1038/nn.2384.

Grand, L., Ftomov, S., and Timofeev, I. (2013). Long-term synchronized electrophysiological and behavioral wireless monitoring of freely moving animals. *J Neurosci Methods* 212**,** 237-241. doi: 10.1016/j.jneumeth.2012.10.008.

Ji, D., and Wilson, M.A. (2007). Coordinated memory replay in the visual cortex and hippocampus during sleep. *Nat Neurosci* 10**,** 100-107. doi: 10.1038/nn1825.

Johnson, L.A., Euston, D.R., Tatsuno, M., and Mcnaughton, B.L. (2010). Stored-trace reactivation in rat prefrontal cortex is correlated with down-to-up state fluctuation density. *J Neurosci* 30**,** 2650-2661. doi: 10.1523/JNEUROSCI.1617-09.2010.

Kandel, E.R. (2001). The molecular biology of memory storage: a dialogue between genes and synapses. *Science* 294**,** 1030-1038. doi: 10.1126/science.1067020.

Karni, A., Tanne, D., Rubenstein, B.S., Askenasy, J.J., and Sagi, D. (1994). Dependence on REM sleep of overnight improvement of a perceptual skill. *Science* 265**,** 679-682.

Kudrimoti, H.S., Barnes, C.A., and Mcnaughton, B.L. (1999). Reactivation of hippocampal cell assemblies: effects of behavioral state, experience, and EEG dynamics. *J Neurosci* 19**,** 4090-4101.

Lancel, M., Van Riezen, H., and Glatt, A. (1991). Effects of circadian phase and duration of sleep deprivation on sleep and EEG power spectra in the cat. *Brain Res* 548**,** 206-214. doi: 0006-8993(91)91123-I.

Loh, D.H., Navarro, J., Hagopian, A., Wang, L.M., Deboer, T., and Colwell, C.S. (2010). Rapid changes in the light/dark cycle disrupt memory of conditioned fear in mice. *PLoS One* 5. doi: 10.1371/journal.pone.0012546.

Luthi, A. (2013). Sleep Spindles: Where They Come From, What They Do. *Neuroscientist*. doi: 10.1177/1073858413500854.

Molle, M., and Born, J. (2011). Slow oscillations orchestrating fast oscillations and memory consolidation. *Prog Brain Res* 193**,** 93-110. doi: 10.1016/B978-0-444-53839-0.00007-7.

Molle, M., Yeshenko, O., Marshall, L., Sara, S.J., and Born, J. (2006). Hippocampal sharp wave-ripples linked to slow oscillations in rat slow-wave sleep. *J Neurophysiol* 96**,** 62-70. doi: 10.1152/jn.00014.2006.

Peyrache, A., Khamassi, M., Benchenane, K., Wiener, S.I., and Battaglia, F.P. (2009). Replay of rule-learning related neural patterns in the prefrontal cortex during sleep. *Nat Neurosci* 12**,** 919-926. doi: 10.1038/nn.2337.

Plihal, W., and Born, J. (1999). Effects of early and late nocturnal sleep on priming and spatial memory. *Psychophysiology* 36**,** 571-582.

Rasch, B., and Born, J. (2013). About sleep's role in memory. *Physiol Rev* 93**,** 681-766. doi: 10.1152/physrev.00032.2012.

Rioult-Pedotti, M.S., Friedman, D., and Donoghue, J.P. (2000). Learning-induced LTP in neocortex. *Science* 290**,** 533-536.

Sakai, T., Tamura, T., Kitamoto, T., and Kidokoro, Y. (2004). A clock gene, period, plays a key role in long-term memory formation in Drosophila. *Proc Natl Acad Sci U S A* 101**,** 16058-16063. doi: 10.1073/pnas.0401472101.

Siapas, A.G., and Wilson, M.A. (1998). Coordinated interactions between hippocampal ripples and cortical spindles during slow-wave sleep. *Neuron* 21**,** 1123-1128.

Sirota, A., Csicsvari, J., Buhl, D., and Buzsaki, G. (2003). Communication between neocortex and hippocampus during sleep in rodents. *Proc Natl Acad Sci U S A* 100**,** 2065-2069. doi: 10.1073/pnas.0437938100.

Smith, C. (1995). Sleep states and memory processes. *Behav Brain Res* 69**,** 137-145.

Tapp, W.N., and Holloway, F.A. (1981). Phase shifting circadian rhythms produces retrograde amnesia. *Science* 211**,** 1056-1058.

Tobler, I., and Borbely, A.A. (1986). Sleep EEG in the rat as a function of prior waking. *Electroencephalogr Clin Neurophysiol* 64**,** 74-76.

Tononi, G., and Cirelli, C. (2003). Sleep and synaptic homeostasis: a hypothesis. *Brain Res Bull* 62**,** 143-150.

Volicer, L., Harper, D.G., Manning, B.C., Goldstein, R., and Satlin, A. (2001). Sundowning and circadian rhythms in Alzheimer's disease. *Am J Psychiatry* 158**,** 704-711.

Wilson, M.A., and Mcnaughton, B.L. (1994). Reactivation of hippocampal ensemble memories during sleep. *Science* 265**,** 676-679.

Witting, W., Kwa, I.H., Eikelenboom, P., Mirmiran, M., and Swaab, D.F. (1990). Alterations in the circadian rest-activity rhythm in aging and Alzheimer's disease. *Biol Psychiatry* 27**,** 563-572.

6. Appendices

The current recording system was designed to conduct LFP recordings in six rats simultaneously for 18 days. Previously groups (Bertram et al., 1997;Grand et al., 2013) have worked to create recording systems capable of recording LFPs for extended periods of time in freely behaving rats. Previously, (Bertram et al., 1997) have described a system of continuously recording LFP and video behaviour (Bertram et al., 1997), but this system can be improved upon with modern digital video recording and electrophysiological techniques. More recently, Grand et al. (2013) have developed a wireless system offering the benefit of having completely untethered animal behaviour, but is limited in continuous recording capability due to the use of a battery power source. For the current study, continuous recordings over 18 days were necessary for observing changes to sleep structure over an acute circadian shift. The current system (supplemental Figure 14) allowed us to monitor the impact of circadian disruption on sleep structure in rodents with the appropriate number of test subjects. This was accomplished by simultaneously recording LFPs from six animals in parallel. Due to the extended and continuous duration of these electrophysiological recordings, this recording system had to be designed to maintain stable recordings. A detailed description of the parts used in the fabrication of this system has been included (supplementary Table 3), which will be referenced for each part in the following appendices. Appendices contain a more detailed description of the methods used in animal preparation and recording system setup for the current experiment.

6.1 Surgical protocol

In preparation for the surgery rats were placed in surgical bedding and housing. Buprenorphine 0.03mL/kg analgesic was administered 30 minutes prior to anesthesia. Rats were then anesthetized using an iso-flurane induction chamber. Rats were then placed onto a heat pad overhead a stereotaxic apparatus, with continued iso-flurane anesthesia. Three pairs of electrodes were subsequently implanted in the hippocampus (-3.84mm from Bregma, 2.4mm lateral with 2.4mm depth, and tip separation of 0.4mm), pre-frontal cortex (2.76mm from Bregma, 2.8mm lateral with 4.25mm depth at a 55^{o} angle from dura, and tip separation of 1.8mm), an EMG sutured bilaterally (on exposed section of EMG electrode loop) to the Acromiotrapezius muscle and a single stainless steel ground screw was also implanted in each rat's cranium (-2mm from Lambda). Electrodes were then pinned into the rat implant connector (Ginder Scientific, Ottawa, ON, Canada) and dental acrylic was used to secure the implant assembly in place. Metacam (Boehringer Ingelheim, St. Joseph, MO, USA) anti-inflammatory agent (0.2 mL/Kg) and Baytril (Bayer, Whippany, NJ, USA) antibiotic (2 mL/Kg) were administered. Following a one to two week recovery period, signal producing inter-cranial LFP electrode to rat tail impedances were tested and ranged from 150K to 400K ohms, EMG electrode impedances ranged from 1K to 5K ohms, and ground screw impedances ranged from 1k to 30k ohms. Depth and positions of electrodes were later confirmed by histological analysis.

6.2 Electrode fabrication

Bi-polar LFP electrodes (supplemental Figure 11), mono-polar EMG electrodes, and animal ground screws were fabricated prior to surgical implantation. Twisted pairs of bipolar electrodes used for inter-cranial LFP recordings (HC and PFC) were constructed from medical grade 40 AWG (American wire gauge) stainless steel wire coated in polytetrafluoroethylene (Teflon) (Sigmund Cohn, Mt Vernon, NY, USA). As a first step, a single strand of stainless steel wire was taken and folded in half (but not creased), twisted at one end, heated over the twisted area with a heat gun to retain the twisted shape, and subsequently cut at the fold to create two lengths of stainless steel wire with one end twisted together. Following this, one end of each wire (opposite the twisted ends) was stripped and crimped into gold pins (Ginder Scientific, Ottawa, ON, Canada). Under a magnifying lens, one of the stainless steel wires was slowly pulled (on the gold pin) while applying slight pressure to the twisted section. By pulling one of the wires we are able to achieve offset electrode tips. The pulled electrode was then marked with a nail polish lacquer, thus marking the shortened electrode of the bi-polar assembly. Bi-polar electrode assembly was then attached to a 22 AWG guide wire (Consolidated Electronic Wire and Cable, Franklin Park, IL, USA) using ultraviolet glue (SDI Limited, Bensenville, IL, USA), in order to increase handling proficiency during surgery. Pre-surgery bi-polar electrode impedances were tested using an impedance meter and recorded ranging from 50K to 100K ohms.

Mono-polar electrodes used for electromyogram (EMG) recordings were also manufactured using stainless steel 40 AWG (Cooner Wire, Chatsworth, CA, USA). A single strand of stainless steel wire was folded, twisted slightly below the folded end to create a small circular loop, and heated over the twisted area with a heat gun to retain twisted shape. Excess wire was then trimmed to the twisted area. Following this, the untrimmed side of the wire was then stripped and crimped into a gold pin (Ginder Scientific, Ottawa, ON, Canada). A section of insulation on the looped end was then removed through exposure to a flame; providing a conductive contact point. Pre-surgery mono-polar electrode impedances were tested using an impedance meter and recorded ranging from 100 to 200 ohms.

Animal ground screws were fabricated using medical grade 40 AWG (American wire gauge) stainless steel wire (Sigmund Cohn, Mt Vernon, NY, USA) and a stainless steel screw (Amazon Supply, Seattle, WA, USA). A segment of stainless steel wire was stripped at one end and soldered to the top of the stainless steel screw. The other end of the stainless steel wire was also stripped and crimped into a gold pin (Ginder Scientific, Ottawa, ON, Canada). Pre-surgery ground screw impedances were tested using an impedance meter and recorded ranging from 1 to 5 ohms.

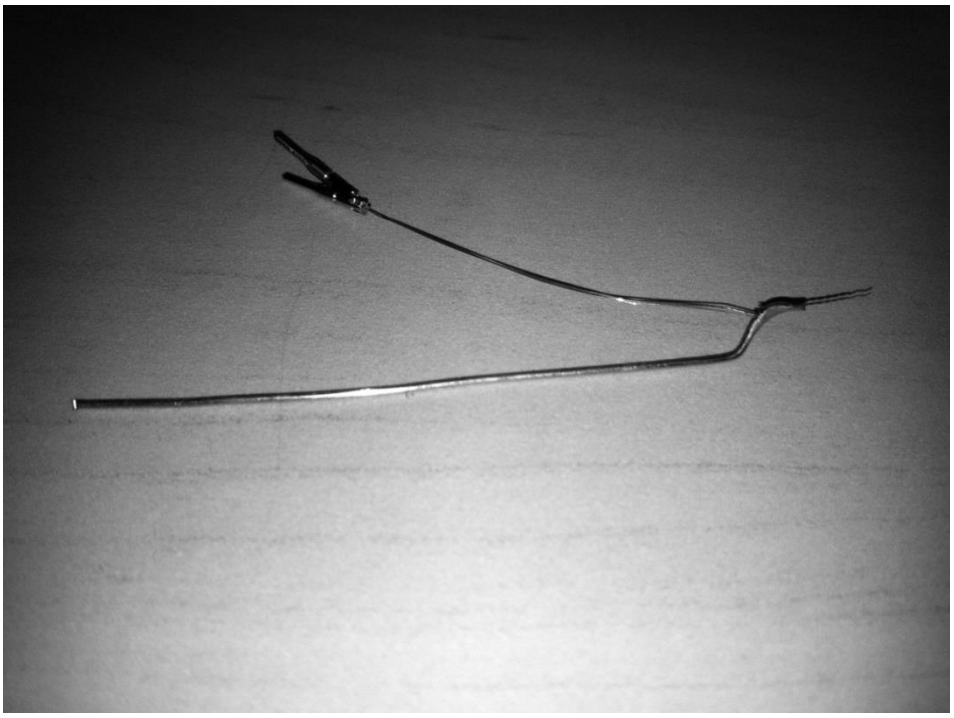

Supplemental Figure 11. Bipolar electrode image, illustrating one bipolar electrode consisting of a twisted pair of single electrodes.

6.3 Tether cable fabrication

Tether cables (supplemental Figure 12) were fabricated from multi-stranded cable (Cooner Wire, Chatsworth, CA, USA). Multiple strands were separated, soldered into gold pins of headstage female connector (Digikey, Thief River Falls, MN, USA), then inserted into connector. The multi-stranded cable wire insulating mesh was also soldered and pinned into the connector as a ground. Subsequently, an epoxy resin was used to solidify connector end assembly. A stainless steel spring (McMaster-Carr, Aurora, OH, USA) was then placed over the multi-stranded cable assembly to improve cable longevity (not shown in supplemental Figure 12). Finally, the commutator male end connector (TEDSS, North Charleston, SC, USA) was soldered onto the other side of the multi-stranded cable; again wire insulating mesh was soldered to the commutator male connector and used as a ground. Heat shrink wrapping was used throughout the soldering process to eliminate cross talk and was also used to hold spring assembly in place over the ends of the cable assembly.

Supplemental Figure 12. Tether cable image, illustrating assembled tether cable components **1**) **and 2)** commutator male end connector, **3) and 4)** headstage female connector.

6.4 Animal to headstage adapter

An adapter (supplemental Figure 13) was fabricated to facilitate a connection between the rat's implant (Ginder Scientific, Ottawa, ON, Canada) and headstage. Wire segments were taken from the multi-stranded tether cable wire (Cooner Wire, Chatsworth, CA, USA), stripped on both sides, and soldered to gold pins (Ginder Scientific, Ottawa, ON, Canada). Gold pins were then inserted into a 9pin socket (Ginder Scientific, Ottawa, ON, Canada). An aluminum ring nut (Ginder Scientific, Ottawa, ON, Canada) was then placed over the 9pin socket (Ginder Scientific, Ottawa, ON, Canada). The remaining stripped ends were then mapped onto a female adapter (Digikey, Thief River Falls, MN, USA), compatible with Neurotek-IT headstages (Neurotek-IT Inc, Toronto, Ontario, Canada). The two connector wiring assembly was then fixed in place using an epoxy resin.

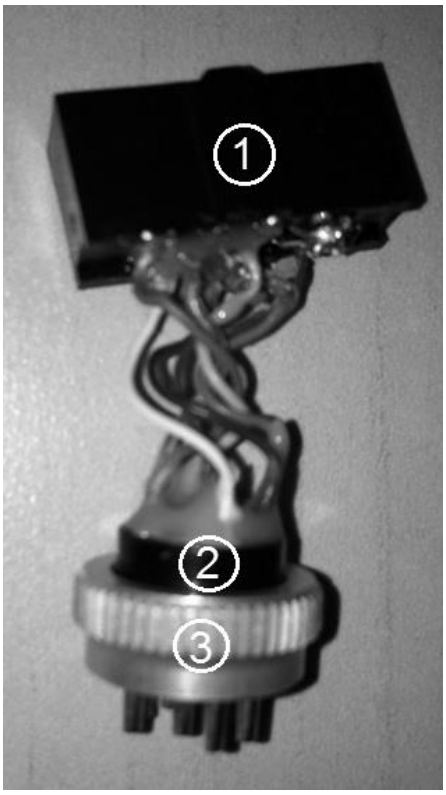

Supplemental Figure 13. Animal to headstage adapter image, illustrating partial assembly of adapter components **1)** female adapter **2)** 9pin socket and **3)** aluminum ring nut.

6.5 Additional figures

Supplemental Figure 14. Recording boxes figure illustrating six animal recording box chambers used in LFP recordings.

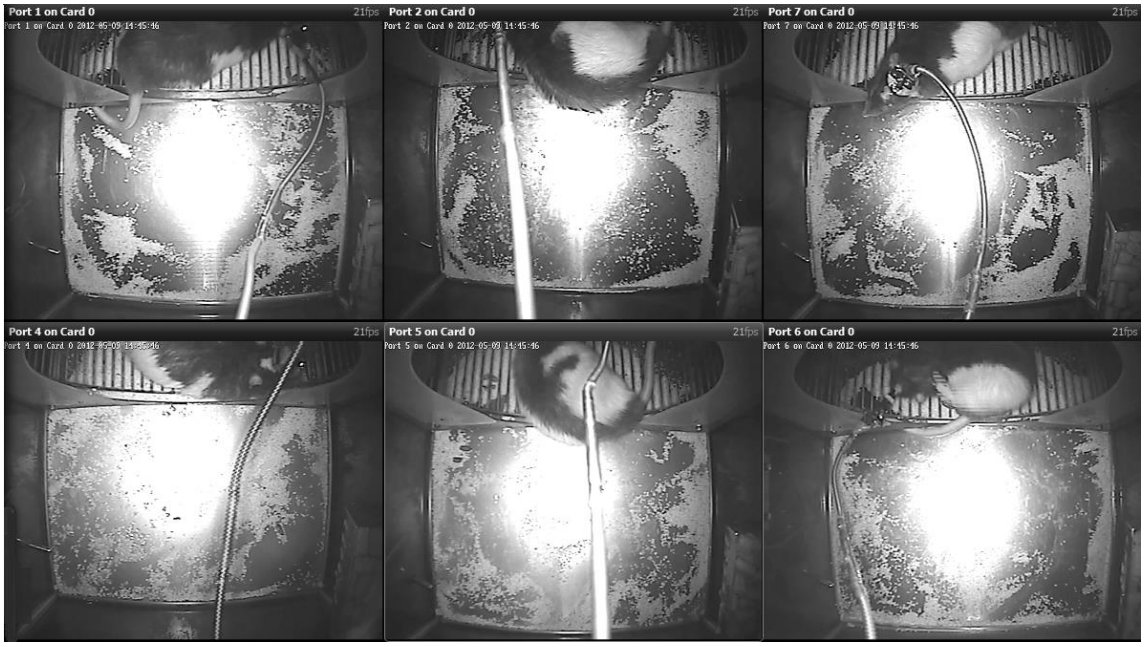

Supplemental Figure 15. Blue Cherry digital video recording system illustrating continuous day and night (infrared) animal monitoring

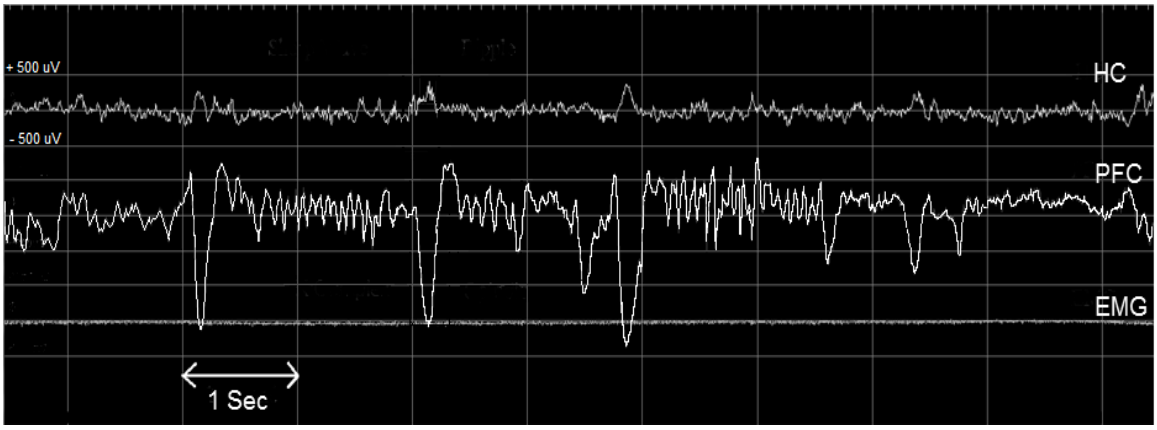

Supplemental Figure 16. EDF Browser representative sample of online LFP monitoring.

Parts List			
Component	**Supplier**	**Product**	**Part Number**
Animal Housing			
• Framing	McMaster-Carr, Aurora, OH, USA	Aluminum t-slotted framing	47065T101
• Corners	McMaster-Carr, Aurora, OH, USA	Aluminum corners	47065T242
• Wheel sensor	Digikey, Thief River Falls, MN, USA	Sensor	HE597-ND
Tether Cable			
• Cable	Cooner Wire, Chatsworth, CA, USA	Tether cable	CW 6005
• Protective spring	McMaster-Carr, Aurora, OH, USA	Spring	9665K84
• Commutator connector	TEDSS, North Charleston, SC, USA	Amphenol connector	126-220
• Headstage connector	Digikey, Thief River Falls, MN, USA	Connector	952-1200-ND
Commutator to Avatar Connector	Multi-Contact, Windsor, CA, USA	Connecting lead	MLK1, 5-BM
Commutator	Crist Instrument Co., Inc	9-Channel commutator	4-TBC-9S
Electrodes			
• Inter-cranial electrode	Sigmund Cohn, Mt Vernon, NY, USA	Stainless steel wire	316SS3T
• Muscle electrode	Cooner Wire, Chatsworth, CA, USA	Stainless steel wire	AS 631
• Cranial guide wire	Consolidated Electronic Wire and Cable, Franklin Park, IL, USA	Tinned copper wire	22 TC, 22 AWG
• Ground screw	Amazon Supply, Seattle, WA, USA	Stainless steel screw	B000FMUH4M
• Ultra violet glue	SDI Limited, Bensenville, IL, USA	Wave	
Surgery			
• Anti-inflammatory	Boehringer Ingelheim, St. Joseph, MO, USA	Metacam	
• Anti-biotic	Bayer, Whippany, NJ, USA	Baytril	
Animal Implant	Ginder Scientific, Ottawa, ON, Canada	Macyntire Melina	GS09
Animal to Headstage Adapter	Digikey, Thief River Falls, MN, USA	Connector	S9194-ND
Electrophysiology			
• EEG recorder	EGI, Eugene, Oregon, USA	Avatar Recorder	
• Headstage	Neurotek-IT Inc, Toronto, Ontario, Canada	8-Channel headstage	
• Headstage and Avatar power supply	Neurotek-IT Inc, Toronto, Ontario, Canada	Power Supply	
Video Recording			
• Digital video card	Bluecherry, Fulton, MO, USA	Hardware compression card	BC-H16480A
• Camera	Bluecherry, Fulton, MO, USA	Infrared dome camera	AGI (VC-CA-DIRR-160)
• Camera power	Bluecherry, Fulton, MO, USA	Power supply	12V DC UL

Supplementary Table 3. Parts list outlining detailed list of components used,